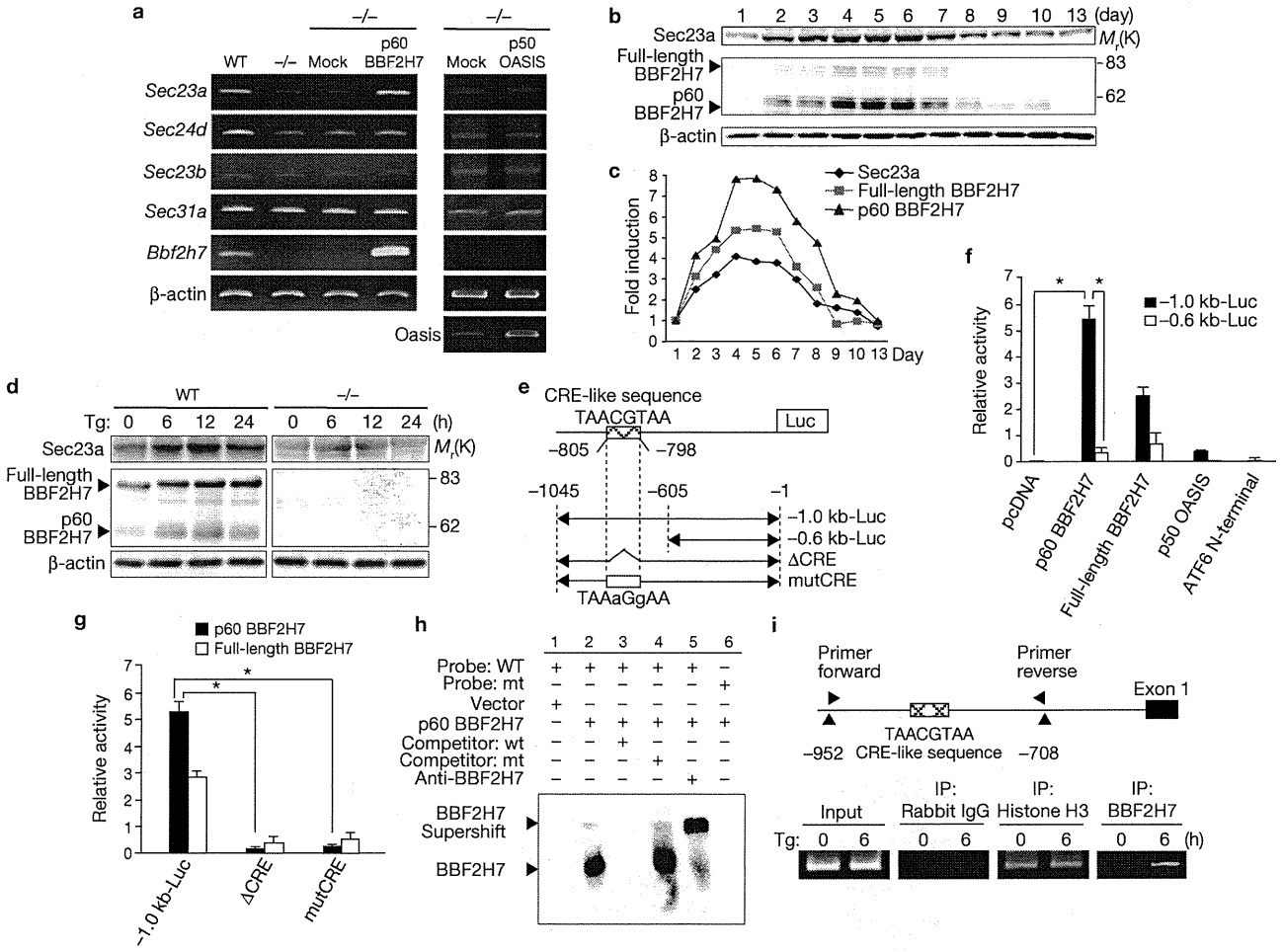

Figure 4 *Sec23a* is a target of BBF2H7. (**a**) RT-PCR analysis using primary cultured chondrocytes. Introduction of p60 BBF2H7 into *Bbf2h7*$^{-/-}$ chondrocytes rescued *Sec23a* expression. Note that OASIS, which is a transcription factor and has a similar structure to BBF2H7, could not rescue *Sec23a* expression. (**b**) Western blotting analysis of Sec23a in mesenchymal cells maintained as a micromass culture. Note that expression of Sec23a proteins at the indicated time points was synchronized with that of BBF2H7. (**c**) Quantitative analysis of Sec23a, full-length BBF2H7 and p60 BBF2H7 protein expression. (**d**) Western blotting analysis using lysates extracted from wild-type (left) and *Bbf2h7*$^{-/-}$ (right) primary cultured chondrocytes exposed to thapsigargin (1 μM; an ER stressor). (**e**) The mouse Sec23a promoter region and reporter plasmids. (**f**) Reporter assays using full-length 1.0-kb and 0.6-kb *Sec23a* promoters. ATDC5 cells were transfected with the indicated constructs and the reporter plasmid pGL3-*Sec23a* promoter (1.0-kb or 0.6-kb) attached to a luciferase gene. The relative luciferase activities in the cells were determined. Data are mean ± s.d., $n = 5$, $^*P < 0.001$(Student's *t*-test). (**g**) Reporter assays of ΔCRE and mutCRE using ATDC5 cells (mean ± s.d., $n = 3$, $^*P < 0.001$(student's *t*-test). (**h**) Gel shift assay shows that the binding of p60 BBF2H7 and the CRE-like sequence was abolished by a competitor (lane 3), and a supershift by an anti-BBF2H7 antibody (lane 5) was detected. (**i**) Chromatin immunoprecipitation assay using primary cultured chondrocytes treated with thapsigargin (1 μM). Top panel, schematic representation of the mouse *Sec23a* promoter and the primer sites. Bottom panel, immunoprecipitation of chromatin with the indicated antibodies. Tg, thapsigargin; Luc, luciferase gene; mt, mutant; IP, immunoprecipitate; WT, wild type; –/–, *Bbf2h7*$^{-/-}$; Mock, empty vector.

reduced secretion of cartilage ECM proteins in *Bbf2h7*$^{-/-}$ cells. The results were consistent with *in vivo* findings from the epiphyseal cartilage in *Bbf2h7*$^{-/-}$ mice. Chondrocyte differentiation requires the attachment of chondrocytes to Col2, in developing bone[17,18]. Thus, pertubation of normal chondrocyte differentiation and cartilage zone formation could be caused by decreased secretion of ECM proteins in *Bbf2h7*$^{-/-}$ mice.

All the ER stress-related genes that we examined were slightly upregulated at days 4 and 7 in micromass culture of wild-type cells (Fig. 3e, f), and chaperone molecules, BiP, PDI and GRP94, were also upregulated (data not shown), indicating that mild ER stress is transiently induced in chondrocytes during their normal differentiation. The expression of ER stress-regulated genes and chaperone molecules in *Bbf2h7*$^{-/-}$ cells was increased compared with that in wild-type cells, and the induction was prolonged until day 13. In the rib cartilage, expression of the ER stress-related genes was also higher in *Bbf2h7*$^{-/-}$ than in wild-type mice (Supplementary Information, Fig. S4). Thus, *Bbf2h7* deficiency causes severe ER stress in chondrocytes, which could be induced by the accumulation of ECM proteins in the ER lumen.

Sox9, which is essential for chondrocyte differentiation[14,19], was highly expressed at days 4 and 7 in the micromass culture (Fig. 3c). *Sox9* expression at these time points could facilitate synthesis of various proteins for chondrocyte differentiation and could induce ER stress in chondrocytes. Reverse transcription (RT)-PCR showed that *Bbf2h7*, *Bip*, *Pdi* and *Grp94* were slightly, but significantly, upregulated by Sox9 (Fig. 3g, h). An active form of BBF2H7, p60 BBF2H7, was obtained

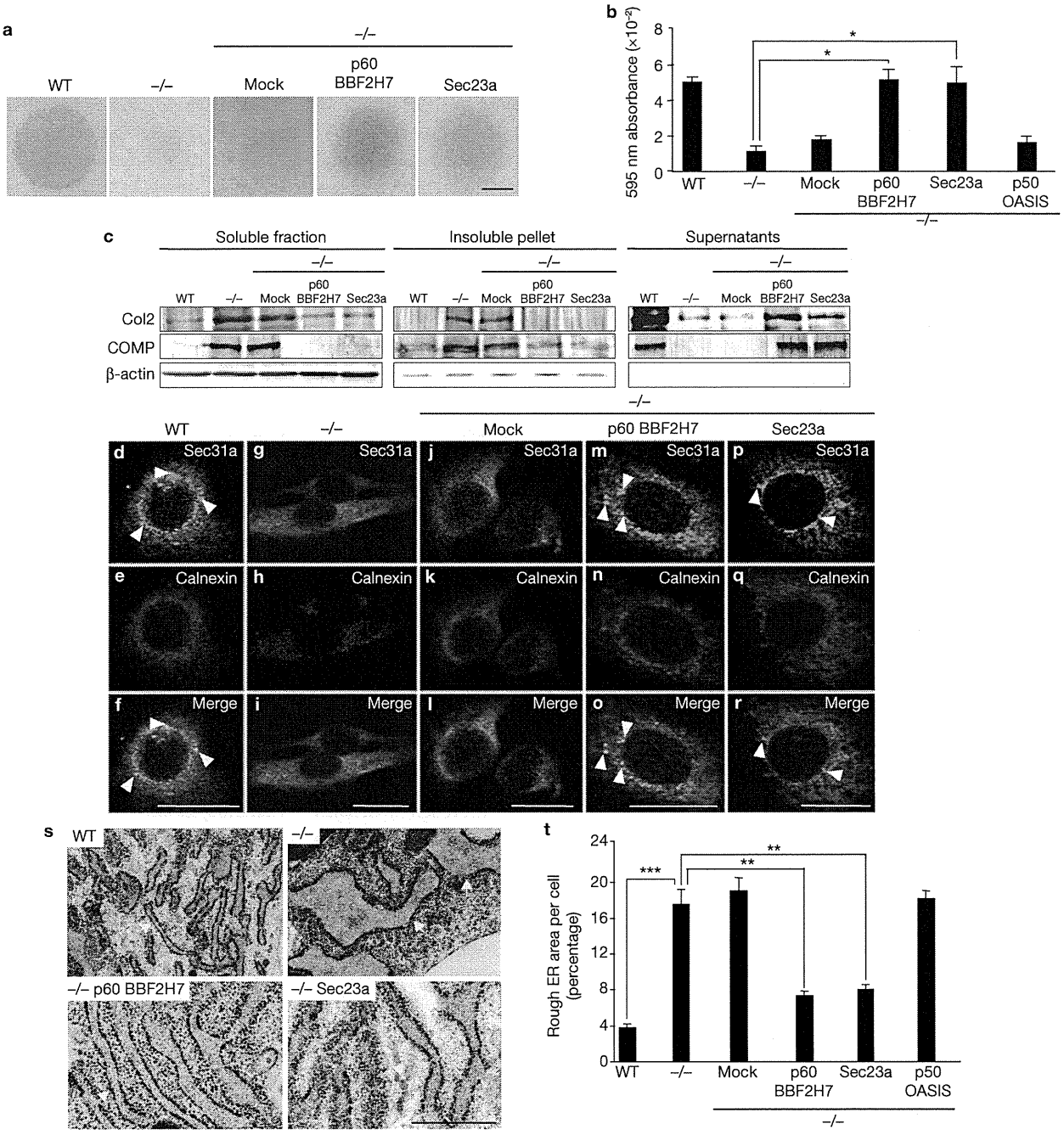

Figure 5 The introduction of Sec23a in *Bbf2h7*$^{-/-}$ cells improves secretion of ECM proteins. (**a**) Mesenchymal cells prepared from wild-type and *Bbf2h7*$^{-/-}$ mice were maintained as micromass cultures for four days, and stained with alcian blue. Infection of *Bbf2h7*$^{-/-}$ cells with an adenovirus expressing p60 BBF2H7 or Sec23a improved the secretion of ECM proteins. Scale bar, 1 mm. (**b**) Quantification of absorbance from cells stained by alcian blue. The introduction of OASIS could not rescue the secretion of ECM proteins in *Bbf2h7*$^{-/-}$ cells. Data are mean ± s.d. $n = 5$, except for *Bbf2h7*$^{-/-}$ *p50* OASIS $n = 3$, $^{*}P < 0.001$ Student's *t*-test. (**c**) Western blotting of Col2 and COMP using lysates extracted from primary cultured chondrocytes in wild-type and *Bbf2h7*$^{-/-}$ mice. Note that the lack of intracellular accumulation of Col2 and COMP, which are secreted into the media by introduction of p60 BBF2H7 or Sec23a into the chondrocytes. (**d–r**) Double-immunofluorescence of Sec31a and calnexin (an ER marker) in primary cultured chondrocytes of wild-type and *Bbf2h7*$^{-/-}$ mice. Arrowheads show punctates of Sec31a recruited to the ER exit site. Scale bars, 20 μm. (**s**) Electron microscopic images of primary cultured chondrocytes from wild-type and *Bbf2h7*$^{-/-}$ mice. Arrows show rough ER. Note disordered parallel stacks of flattened cisternae in *Bbf2h7*$^{-/-}$ chondrocytes infected with Sec23a. Scale bars, 0.5 μm. (**t**) Two-dimensional analysis of rough ER area using electron micrographs. The introduction of OASIS could not improve the size of the rough ER in *Bbf2h7*$^{-/-}$ chondrocytes. Mean ± s.d., $n = 20$, except for *Bbf2h7*$^{-/-}$ OASIS $n = 5$; $^{**}P < 0.05$, $^{***}P < 0.01$ (Student's *t*-test). WT, wild type; −/−, *Bbf2h7*$^{-/-}$; Mock, empty vector.

in response to *Sox9* expression by western blotting analysis (Fig. 3i). Therefore, *Sox9* could induce mild ER stress and activate BBF2H7 during chondrocyte differentiation.

We compared gene expressions in primary cultured chondrocytes prepared from the rib cartilage of wild-type and *Bbf2h7*$^{-/-}$ mice at E18.5 using a microarray. Various genes associated with the protein secretory

pathway and ER biogenesis were significantly downregulated in *Bbf2h7*$^{-/-}$ chondrocytes (Supplementary Information, Fig. S5a). Among these genes, which are directly or indirectly controlled by BBF2H7, *Sec23a* was the most downregulated. RT-PCR showed that *Sec23a* was 80% downregulated, but the expression of the other genes encoding components of the COPII vesicle was not changed (Fig. 4a). Western blotting (Supplementary Information, Fig. S5b) and immunofluorescence (Supplementary Information, Fig. S5c) also showed that Sec23a is significantly decreased in *Bbf2h7*$^{-/-}$ chondrocytes. We infected primary cultured chondrocytes prepared from *Bbf2h7*$^{-/-}$ mice with an adenovirus expressing p60 BBF2H7. *Sec23a* was significantly upregulated by overexpression of p60 BBF2H7, but expression of the other genes, including components of the COPII vesicle, were not affected (Fig. 4a; Supplementary Information, Fig. S5d). An active form of OASIS (p50 OASIS), which is structurally very similar to BBF2H7 and is expressed in osteoblasts and astrocytes[6], could not induce *Sec23a* expression, indicating that *Sec23a* induction by BBF2H7 is specific.

In a micromass culture at day 1, *Sec23a* expression was relatively low (Fig. 4b, c). This signal markedly increased from day 2 to 6, before decreasing. The expression pattern of *Sec23a* was very similar to that of *BBF2H7* (Fig. 4b, c). As BBF2H7 is activated in response to ER stress[1], if *Sec23a* is a direct target of BBF2H7, *Sec23a* should be induced in chondrocytes undergoing ER stress. Indeed, in primary cultured chondrocytes of wild-type mice, *Sec23a* was markedly induced during ER stress, which was synchronized with the activation of BBF2H7 (Fig. 4d). In contrast, the induction of *Sec23a* was significantly attenuated in *Bbf2h7*$^{-/-}$ chondrocytes. These findings strongly indicate that *Sec23a* is a direct target of BBF2H7.

To identify the cis-acting element in the *Sec23a* promoter region that is responsive to BBF2H7, we searched within 2-kb upstream of the *Sec23a* transcription start site, using the TFSEARCH (http://mbs.cbrc.jp/research/db/TFSEARCH.html). We found a CRE (cAMP-responsive element)-like sequence (5′-TAACGTAA-3′, −805 to −798 base pairs) that is conserved among human, mouse and rat. We previously reported that BBF2H7 can bind to CRE (5′-TGACGTTT-3′) and promote transcription[1]. We performed reporter assays using a reporter gene carrying a 1-kb and a 0.6-kb promoter region of *Sec23a* (Fig. 4e). In cells transfected with a 1-kb reporter construct, reporter activity was significantly induced by introduction of an expression vector for full-length BBF2H7 or p60 BBF2H7 (Fig. 4f). However, reporter activity was rarely induced by BBF2H7 in cells transfected with a 0.6-kb reporter construct. Moreover, reporter activity in cells transfected with 1.0-kb *Sec23a* promoter region lacking, or containing a mutated, CRE-like sequence (ΔCRE and mutCRE, respectively) was dramatically reduced (Fig. 4g).

To confirm that BBF2H7 directly binds to the CRE-like sequence, we performed electrophoretic mobility shift assays (EMSAs). p60 BBF2H7 bound to the CRE-like sequence (Fig. 4h). This binding was abolished by incubation with a 100-fold excess of unlabelled competitors, but not by mutated competitors. The addition of an anti-BBF2H7 antibody caused a supershift (Fig. 4h). Furthermore, we carried out a chromatin immunoprecipitation (ChIP) assay (Fig. 4i). A high level of BBF2H7 binding to the endogenous *Sec23a* promoter was detected in chondrocytes exposed to ER stress. We conclude that BBF2H7 directly binds to the CRE-like sequence within the *Sec23a* promoter region and facilitates its transcription, in chondrocytes.

Sec23a has crucial roles in COPII vesicle formation and anterograde transport of cargo proteins from the ER to the Golgi[3]. Therefore, abnormal cartilage formation involving disturbed secretion of ECM proteins and aggregation of Col2 and COMP in the ER lumen in *Bbf2h7*$^{-/-}$ mice could be associated with decreased *Sec23a* expression, in chondrocytes. In micromass-cultured *Bbf2h7*$^{-/-}$ cells infected with an adenovirus expressing p60 BBF2H7 or Sec23a, secretion of ECM proteins significantly increased and alcian blue ECM-positive contents recovered to the level of those in wild-type cells (Fig. 5a, b). In primary cultured *Bbf2h7*$^{-/-}$ chondrocytes infected with p60 BBF2H7 or Sec23a, the intracellular accumulation of Col2 and COMP completely ceased, and these ECM proteins were secreted into the media as with wild-type chondrocytes (Fig. 5c).

Sec23a recruits other components of the COPII vesicle, including Sec31, and completes the complex before transporting secretory proteins from the ER to the Golgi[2,3]. A mutation of *Sec23a* causes cranio-lenticulo-sutural dysplasia (CLSD), which is characterized by a malformed craniofacial structure involving chondrodysplasia, and cataracts[20]. The mutation reduces the affinity of the Sec13–Sec31 complex[20]. Hence, we examined the localization of Sec31 in primary cultured chondrocytes of *Bbf2h7*$^{-/-}$ mice. Sec31a showed a punctate localization surrounding the ER, which is assumed to recruit to the exit site of the ER membrane in wild-type chondrocytes (Fig. 5d, f). In *Bbf2h7*$^{-/-}$ chondrocytes, Sec31a was diffusely localized in the cytosol and the punctate localization surrounding the ER was not observed (Fig. 5g, i). This mislocalization of Sec31a was rescued by the overexpression of p60 BBF2H7 (Fig. 5m, o) or Sec23a (Fig. 5p, r).

In addition to the disturbance of ECM protein secretion, drastic expansion of the rough ER was observed in *Bbf2h7*$^{-/-}$ chondrocytes (Fig. 2a). We examined ultrastructural changes of rough ER in *Bbf2h7*$^{-/-}$ chondrocytes infected with p60 BBF2H7 or Sec23a (Fig. 5s). The two-dimensional size of the rough ER in *Bbf2h7*$^{-/-}$ chondrocytes infected with p60 BBF2H7 or Sec23a was obtained (Fig. 5s,t). However, *Bbf2h7*$^{-/-}$ chondrocytes infected with Sec23a showed disordered parallel stacks of flattened cisternae that were not completely rescued, this was in contrast to the effect of p60 BBF2H7 introduction. As shown in the microarray data, many other genes, including ER biogenesis-related genes, are also under BBF2H7 control. Therefore, those genes could also be necessary for the complete rescue of *Bbf2h7*$^{-/-}$ chondrocytes. Taken together, these results indicate that perturbance of ER to Golgi trafficking and reduced secretion of ECM proteins are directly due to *Bbf2h7* deficiency and that a BBF2H7-mediated Sec23a pathway is essential for the ER stress-coupled vesicle transport system in chondrocytes.

Sec23b, which is paralogous to Sec23a, functions commutatively with Sec23a to prevent disruption of the secretory pathway. The localization of Sec23b in tissue is different from that of Sec23a[21]. The expression level of Sec23b in chondrocytes is very low; it is much higher in fibroblasts (Supplementary Information, Fig. S6a). In *Bbf2h7*$^{-/-}$ fibroblasts, the ER showed only a slight expansion of its lumen (Supplementary Information, Fig. S6b). Therefore, Sec23b is presumed to be sufficient to compensate for the downregulation of Sec23a in *Bbf2h7*$^{-/-}$ fibroblasts. The severe pathology in the cartilage of *Bbf2h7*$^{-/-}$ mice could be explained by insufficient availability of Sec23b to provide normal Sec23 function.

ER stress markers are mildly upregulated during chondrocyte differentiation in micromass cultures and primary cultures of chondrocytes. Moreover, BBF2H7 is highly cleaved at its membrane region in response to stimulation of differentiation by Sox9, indicating that ER stress is induced during normal chondrocyte differentiation.

Chondroprogenitor cells synthesize relatively low levels of matrix proteins. On differentiation into chondrocytes, abundant cartilage matrix proteins are produced, increasing the burden on the ER. The BBF2H7–Sec23a pathway improves the ER lumen environment by accelerating trafficking from the ER to the Golgi, followed by smooth secretory protein transport. The signalling mediated by BBF2H7 is essential for chondrocyte differentiation and formation of epiphyseal cartilage (Supplementary Information, Fig. S6c). This study has expanded our view of the ER stress response, which deals with unfolded proteins accumulated in the ER to protect against cellular damage, to include activating trafficking to secrete abundant matrix proteins during chondrogenesis. □

METHODS

Methods and any associated references are available in the online version of the paper at http://www.nature.com/naturecellbiology/.

Note: Supplementary Information is available on the Nature Cell Biology website.

ACKNOWLEDGEMENTS

We thank M. Tohyama and S. Shiosaka for helpful discussions and critical reading of the manuscript, and K. Ogawa, A. Ikeda, I. Tsuchimochi, T. Kawanami, A. Kawai and Y. Koreeda for technical support. This work was partly supported by grants from the Japan Society for the Promotion of Science KAKENHI (#19659082, #20059028, #19790238 and #20-3757) and The Novartis Foundation (Japan) for the Promotion of Science.

AUTHOR CONTRIBUTIONS

A.S. and K.I. designed experiments. A.S., S.H., T.M., S.Ka and S.Ko performed experiments. M.S., R.N., T.Y., T.F. and S.I. guided cartilage experiments. S.H., M.I. and M.O. generated *Bbf2h7*$^{-/-}$ mice. R.N., T.Y., S.I. and M.O. helped write the manuscript. A.S. and K.I. wrote the manuscript. K.I. supervised the project.

COMPETING FINANCIAL INTERESTS

The authors declare no competing financial interests.

Published online at http://www.nature.com/naturecellbiology/.
Reprints and permissions information is available online at http://npg.nature.com/reprintsandpermissions/.

1. Kondo, S. *et al.* BBF2H7, a novel transmembrane bZIP transcription factor, is a new type of endoplasmic reticulum stress transducer. *Mol. Cell. Biol.* **27,** 1716–1729 (2007).
2. Paccaud, J. P. *et al.* Cloning and functional characterization of mammalian homologues of the COPII component Sec23. *Mol. Biol. Cell* **7,** 1535–1546 (1996).
3. Fromme, J. C., Orci, L. & Schekman, R. Coordination of COPII vesicle trafficking by Sec23. *Trends Cell Biol.* **98,** 330–336 (2008).
4. Ron, D. Translational control in the endoplasmic reticulum stress response. *J. Clin. Invest.* **110,** 1383–1388 (2002).
5. Schroder, M. & Kaufman, R. J. ER stress and the unfolded protein response. *Mutat. Res.* **569,** 29–63 (2005).
6. Kondo, S. *et al.* OASIS, a CREB/ATF-family member, modulates UPR signalling in astrocytes. *Nature Cell Biol.* **7,** 186–194 (2005).
7. Murakami, T. *et al.* Cleavage of the membrane-bound transcription factor OASIS in response to endoplasmic reticulum stress. *J. Neurochem.* **96,** 1090–1100 (2006).
8. Omori, Y. *et al.* CREB-H: a novel mammalian transcription factor belonging to the CREB/ATF family and functioning via the box-B element with a liver-specific expression. *Nucleic Acids Res.* **29,** 2154–2162 (2001).
9. Zhang, K. *et al.* Endoplasmic reticulum stress activates cleavage of CREBH to induce a systemic inflammatory response. *Cell* **124,** 587–599 (2006).
10. Adham, I. M. *et al.* Reduction of spermatogenesis but not fertility in Creb3l4-deficient mice. *Mol. Cell. Biol.* **25,** 7657–7664 (2005).
11. Nagamori, I. *et al.* The testes-specific bZip type transcription factor Tisp40 plays a role in ER stress responses and chromatin packaging during spermiogenesis. *Genes Cells* **11,** 1161–1171 (2006).
12. Lu, R., Yang, P., O'Hare, P. & Misra, V. Luman, a new member of the CREB/ATF family, binds to herpes simplex virus VP16-associated host cellular factor. *Mol. Cell. Biol.* **17,** 5117–5126 (1997).
13. Chen, Q., Johnson, D. M., Haudenschild, D. R. & Goetinck, P. F. Progression and recapitulation of the chondrocyte differentiation program: cartilage matrix protein is a marker for cartilage maturation. *Dev. Biol.* **172,** 293–306 (1995).
14. Kronenberg, H. M. Developmental regulation of the growth plate. *Nature* **423,** 332–336 (2003).
15. Cremer, M. A., Rosloniec, E. F. & Kang, A. H. The cartilage collagens: a review of their structure, organization, and role in the pathogenesis of experimental arthritis in animals and in human rheumatic disease. *J. Mol. Med.* **76,** 275–288 (1998).
16. Oldberg, A., Antonsson, P., Lindblom, K. & Heinegård, D. COMP (cartilage oligomeric matrix protein) is structurally related to the thrombospondins. *J. Biol. Chem.* **267,** 22346–22350 (1992).
17. Terpstra, L. *et al.* Reduced chondrocyte proliferation and chondrodysplasia in mice lacking the integrin-linked kinase in chondrocytes. *J. Cell Biol.* **162,** 139–148 (2003).
18. Bengtsson, T. *et al.* Loss of alpha10beta1 integrin expression leads to moderate dysfunction of growth plate chondrocytes. *J. Cell Sci.* **118,** 929–936 (2005).
19. Bi, W., Deng, J. M., Zhang, Z., Behringer, R. R. & de Crombrugghe, B. Sox9 is required for cartilage formation. *Nature Genet.* **22,** 85–89 (1999).
20. Boyadjiev, S. A. *et al.* Cranio-lenticulo-sutural dysplasia is caused by a *SEC23A* mutation leading to abnormal endoplasmic-reticulum-to-Golgi trafficking. *Nature Genet.* **38,** 1192–1197 (2006).
21. Fromme, J. C. *et al.* The genetic basis of a craniofacial disease provides insight into COPII coat assembly. *Dev. Cell* **13,** 623–634 (2007).

METHODS

Generation of *Bbf2h7*$^{-/-}$ mice. A targeting vector containing a a neomycin-resistant gene was used to generate *Bbf2h7*$^{-/-}$ (Supplementary Information Fig. S1a). The *Bbf2h7* targeting vector was electroporated into embryonic stem (ES) cells derived from 129/Sv (D3) mice. Homologous recombination was identified by genomic PCR and Southern blotting. The primers used for the PCR were: 5′-CTGCAGTGGTCAGATGGACAG-3′ (common forward), 5′-TGGCTGCGCTGCTGCCCAAGACCCAG-3′ (wild-type reverse) and 5′-CTTGACGAGTTCTTCTGAGG-3′ (targeting reverse). Germ-line transmission of the mutant allele was achieved using C57BL/6 mice. All experiments were performed with the consent of the Animal Care and Use Committee of Miyazaki University and Osaka University.

Cell culture and adenovirus infection. Primary cultured chondrocytes were prepared from rib cartilage of E18.5 wild-type and *Bbf2h7*$^{-/-}$ mice, using a modification of previously published protocols[22]. Briefly, chondrocytes were isolated using 0.2% collagenase D (Roche) after adherent connective tissue had been removed by 0.2% trypsin (Sigma) and collagenase pretreatment. Isolated chondrocytes were maintained in α-MEM (Gibco) supplemented with 10% FCS and ascorbic acid (50 μg ml^{-1}).

Micromass culture was modified according to previously published protocols[23]. Briefly, mesenchymal cells were prepared from the limbs of E11.5 mice and digested with 0.1% trypsin and 0.1% Collagenase D. A total of 1×10^7 cells ml^{-1} were plated and maintained in α-MEM supplemented with BMP-2 (100 ng ml^{-1}; Sigma), ascorbic acid (50 μg ml^{-1}) and β-glycerophosphate (5 nM). ATDC5, a murine chondrogenic cell line, was obtained from RIKEN Cell Bank and cultured in α-MEM supplemented with 10% FCS and ITS solution (Sigma).

Primary cultured fibroblasts were prepared from skin of E18.5 wild-type and *Bbf2h7*$^{-/-}$ mice. The skin was digested with 0.25% trypsin. Isolated fibroblasts were maintained in D-MEM (Gibco) supplemented with 10% FCS.

The recombinant adenovirus carrying mouse HA-Sox9 was generated as described previously[24]. Adenovirus vectors expressing mouse p60 BBF2H7 (1-377 aa), Sec23a and OASIS were constructed with the AdenoX Expression system (Clontech), according to the manufacturer's protocol. Cells were infected with adenoviruses 30 h before analysis.

Antibodies. An anti-BBF2H7 antibody was generated as described previously[1]. For immunohistochemistry, the following antibodies were used: anti-Col2 (Acris Antibodies GmbH; 1:50), anti-COMP (Kamiya Biomedical; 1:100), anti-KDEL (MBL; 1:100) and anti-PCNA (Santa Cruz Biotechnology; 1:100). For western blotting (WB) and immunofluorescence, the following antibodies were used: anti-β-actin (WB 1:3,000), anti-Sec23a (Sigma; WB 1:1,000), anti-Col2 (Acris Antibodies GmbH; WB 1:500), anti-COMP (Kamiya Biomedical; WB 1:500), anti-Calnexin, anti-Phospho-eIF2α (StressGen Biotechnologies; WB 1:1,000), anti-Sec31a (BD Transduction Laboratories), anti-ATF4 (Santa Cruz Biotechnology; WB 1:1,000), anti-BiP (WB 1:1,000), anti-PDI (MBL; WB 1:1,000), anti-Caspase 3 (Cell Signaling; WB 1:1,000) and anti-Sec23b (Abcam; WB 1:1,000). For immunofluoresence all antibodies were used at a 1:500 dilution.

Histological and immunohistochemical analysis and immunofluorescence. For histological analysis, limbs were fixed in 10% formalin and then decalcified with 10% EDTA. hematoxylin-eosin and toluidine blue staining were performed using paraffin sections (6 μm) according to standard protocols. For immunohistochemistry, limbs were fixed in 4% paraformaldehyde (PFA) and then decalcified with Morse's solution. Frozen sections (10 μm) were digested with pepsin (1 mg ml^{-1}; Wako) in HCl (0.1 N; for the detection of Col2 and COMP). Cells were visualized under a fluorescence microscope or a confocal microscope (Olympus FV1000D). For immunofluorescence, cells were fixed in cold methanol and then permeabilized in 0.5% Triton-X 100. Cells were visualized under a confocal microscope (Olympus FV1000D).

RT-PCR and *in situ* hybridization. RT-PCR was performed using each specific primer set (Supplementary Information, Table S1). The density of each band was quantified using the Adobe Photoshop Elements 2.0 Program (Adobe Systems Incorporated). For *in situ* hybridization using digoxigenin-labelled probes (Supplementary Information, Table 2), limbs were fixed in 4% PFA and then decalcified with Morse's solution. The frozen sections (10 μm) were digested with proteinase K, and fixed in 4% PFA followed by acetylation.

Electron microscopy. For histological analysis, limbs were fixed in 2.5% glutaraldehyde, decalcified in a 10% EDTA–Na_2, and post-fixed in 2% osmium tetroxide. Pancreases were isolated from wild-type and *Bbf2h7*$^{-/-}$ mice at E18.5 and electron microscopy was performed as described previously[25]. For analysis of cultured cells, cells were fixed in 2.5% and glutaraldehyde, 2% PFA and post-fixed in 2% osmium tetroxide. After dehydration, they were embedded in EPON812. Ultrathin sections were stained with uranyl acetate and lead citrate. They were visualized using a Hitachi 7100 electron microscope operated at 80 kV. The mean cell area was determined using ImageJ software (NIH).

Alcian blue and alizarin red staining. For staining of skeletons, E18.5 mice were eviscerated and fixed in 95% ethanol, followed by alcian blue (Merck) and alizarin red (Sigma) staining. For micromass cultures, cells were stained as described previously[23]. Briefly, cells were fixed in cold methanol, and washed with HCl (0.1 N; pH 1.0). After staining in 1% alcian blue or 0.5% alizarin red, alcian blue and alizarin red stains were solubilized with guanidine hydrochloride (6 M) and cetylpyridinium chloride (100 mM), respectively. Absorbance was measured using a spectrophotometer at 595 nm (alcian blue stain) and 570 nm (alizarin red stain).

Microarray analysis. Experimental sample RNAs were isolated using RNeasy (Qiagen) and analysed using Mouse Genome 430 2.0 Array (Miyazaki Prefectural Industrial Support Foundation and Affymetrix) and Mouse Oligo chip 24K 3D-Gene (Toray).

Fractionation. The detergent-soluble/insoluble fractionations were modified from a protocol described previously[26]. Supernatants were concentrated using a Microcon filter (Millipore). The protein concentration was equalized using bicinchoninic acid (BCA) protein assay reagents (Pierce).

Luciferase assay. ATDC5 cells were plated and transfected with a reporter plasmid (0.2 μg) carrying the firefly luciferase gene, a reference plasmid pRL-SV40 (0.02 μg) carrying the *Renilla* luciferase gene under the control of the SV40 enhancer and promoter (Promega) and an effector protein expression plasmid (0.2 μg), using FuGene 6 (Roche). After 24 h, luciferase activities were measured using Dual-Luciferase Reporter Assay System (Promega) and a luminometer (Berthold Technologies), according to the manufacturer's protocol. Relative activity was defined as the ratio of firefly luciferase activity to that of *Renilla* luciferase.

Electrophoretic mobility shift and chromatin immunoprecipitation assays. The electrophoretic mobility shift assay was performed as described previously[6]. For supershift experiments, samples were treated with an anti-BBF2H7 antibody at 4 °C for 1 h before incubation with a radiolabelled probe. The sequences of the oligonucleotides used in the binding were: 5′-TCTACAG TTTGCAGTGTAACGTAAGCTGGGCTGCCTTTTT-3′ (CRE-wild-type) and 5′-TCTACAGTTTGCAGTGTAAaGgAAGCTGGGCTGCCTTTTT-3′ (CRE-mutant). The chromatin immunoprecipitation assay was performed as described previously[6]. The primers used for the mouse *Sec23a* promoter were: 5′-CTCATTAGGTAGCTCAAGGAGTCTC-3′ (forward) and 5′-CACTCGGCT AGTGGTGATGGTTCATG-3′ (reverse), yielding a 245-base pair product.

Accession number of microarray data. The complete microarray data are available in Gene Expression Omnibus (GEO; accession number, GSE18052).

22. Muramatsu, S. *et al.* Functional gene screening system identified *TRPV4* as a regulator of chondrogenic differentiation. *J. Biol. Chem.* **282,** 32158–32167 (2007).
23. Woods, A., Khan, S. & Beier, F. C-type natriuretic peptide regulates cellular condensation and glycosaminoglycan synthesis during chondrogenesis. *Endocrinology* **148,** 5030–5041 (2007).
24. Hata, K. *et al.* Paraspeckle protein p54nrb links Sox9-mediated transcription with RNA processing during chondrogenesis in mice. *J. Clin. Invest.* **118,** 3098–3108 (2008).
25. Heather, P. *et al.* Diabetes mellitus and exocrine pancreatic dysfunction in perk-/- mice reveals a role for translational control in secretory cell survival. *Mol. Cell* **7,** 1153–1163 (2001).
26. Imai, Y. *et al.* An unfolded putative transmembrane polypeptide, which can lead to endoplasmic reticulum stress, is a substrate of Parkin. *Cell* **105,** 891–902 (2001).

nature
cell biology

DOI: 10.1038/ncb1962

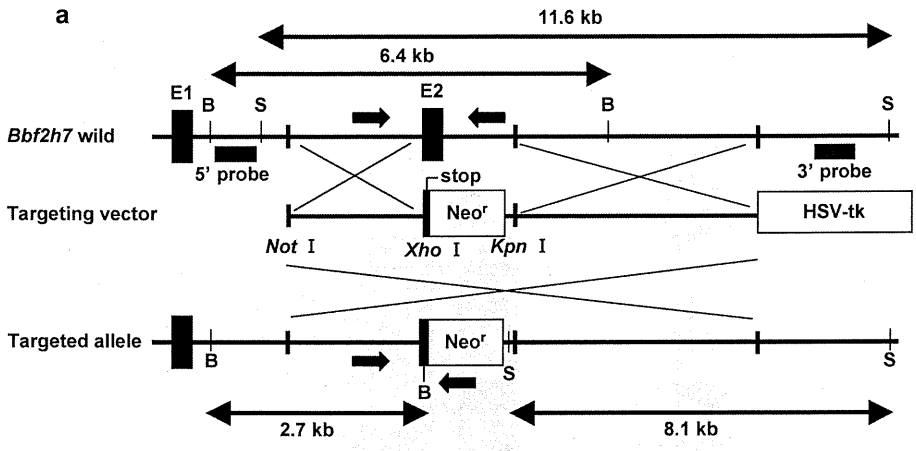

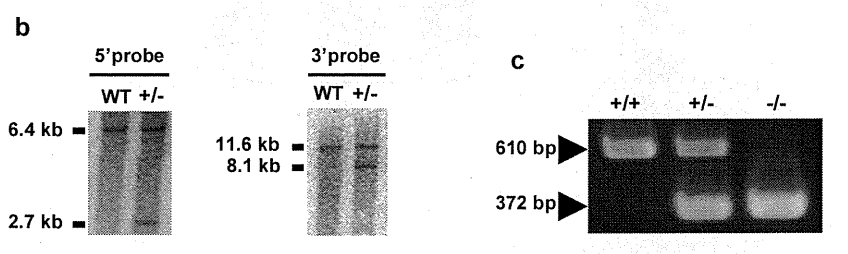

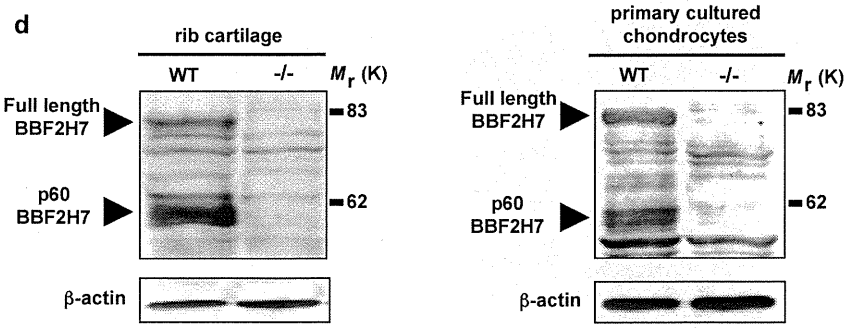

e

Age	Total	+/+	+/-	-/-
E11.5	170	51	81	38
E14.5	48	13	24	11
E16.5	42	10	23	9
E18.5	671	169	315	187

Figure S1 Generation of *Bbf2h7-/-* mice. (**a**) Targeted disruption of the mouse *Bbf2h7* gene. Schematic representations of the wild type *Bbf2h7* allele, the targeting vector and the predicted *Bbf2h7* targeted allele. Black boxes indicate the exons of the *Bbf2h7*, white boxes indicate PGK-neo cassette and HSV-tk cassette. The positions of the primer pairs used for genotype are denoted by small opposing arrows. The positions of the external probes used for Southern blot are indicated by the small black boxes. B: BamHI, S: SphI. (**b**) Southern blotting of WT and heterozygous (+/-) ES cells. A 5'-external probe recognizes 6.4 kb wild type and 2.7 kb targeted BamHI DNA fragments (left). A 3'-external probe recognizes 11.6 kb wild type and 8.1 kb targeted SphI DNA fragments (right). (**c**) Genotyping of wild type (+/+), heterozygous (+/-), and homozygous (-/-) mice by PCR. The wild type allele is identified by the 610 bp product and the targeted allele is identified by the 372 bp product. (**d**) Western blotting of lysates extracted from embryonic day (E) 18.5 rib cartilage (left) and primary cultured chondrocytes (right). (**e**) Wild-type (+/+), heterozygous (+/-), and homozygous (-/-) mice were obtained in the expected Mendelian ratio.

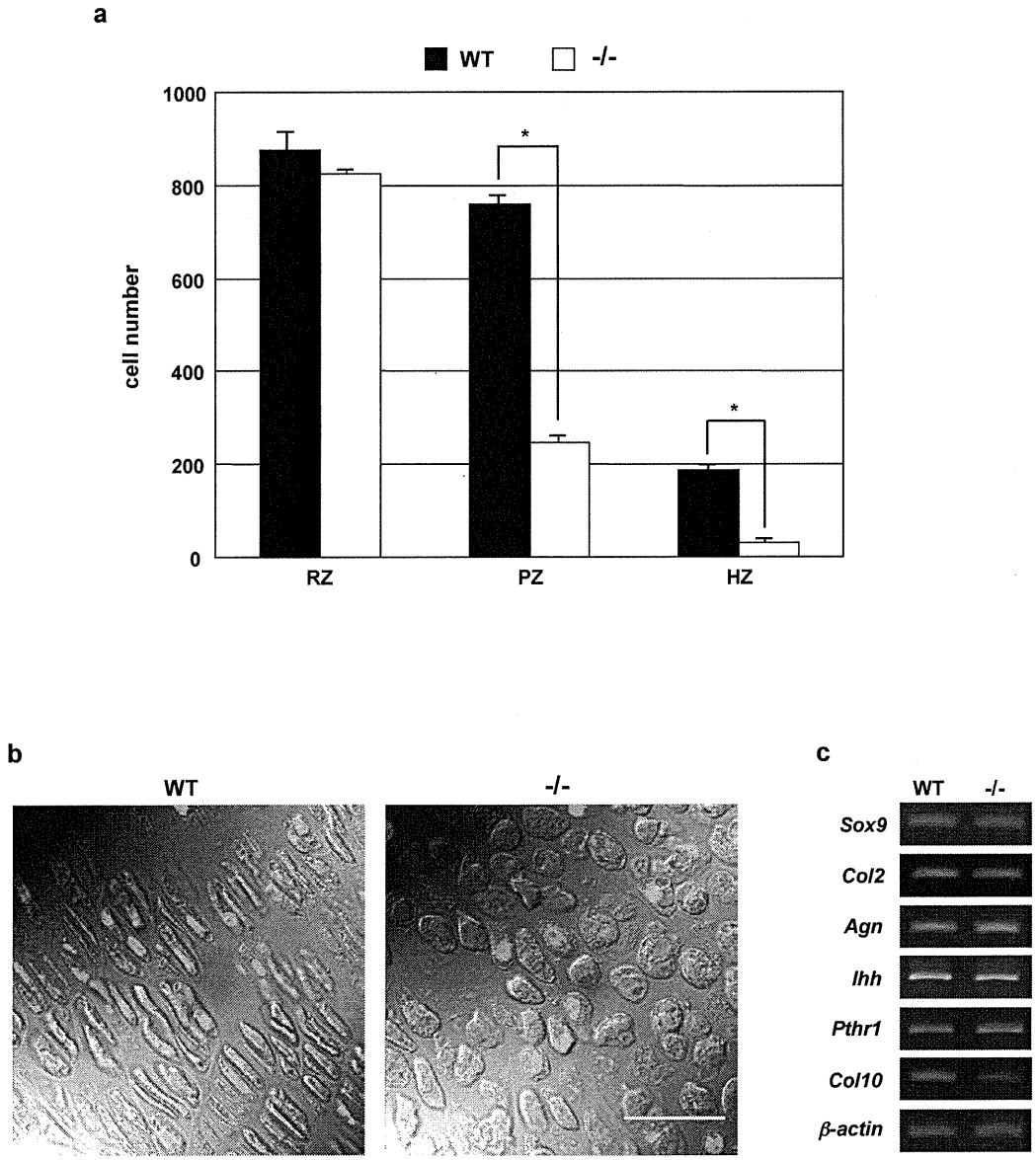

Figure S2 The proliferating and hypertrophic zone was reduced in *Bbf2h7-/-* mice cartilage. (**a**) Hematoxylin-Eosin (HE) stained cartilage in the tibia of WT and *Bbf2h7-/-* mice at E18.5 was visualized under a microscope. The borders of each zone were manually defined and cells were counted. RZ: resting zone, PZ: proliferating zone, HZ: hypertrophic zone (mean ± SD, N=4, *p<0.05, student's t-test). (**b**) Immunohistochemical analysis of proliferating cell nuclear antigen (PCNA), which is a marker for proliferating cells, in the proliferating zone of tibia at E18.5 of WT and *Bbf2h7-/-* mice. Although the proliferating chondrocytes in *Bbf2h7-/-* mice exhibited abnormal morphology, positive signals for PCNA were detected in those cells. Bar: 50 μm. (**c**) Messenger RNA was extracted from E18.5 rib cartilage of WT and *Bbf2h7-/-* mice. The expression levels of those markers except for *type X collagen* (*Col10*) in *Bbf2h7-/-* mice were almost similar to those in WT mice. The *Col10* expression was significantly reduced in *Bbf2h7-/-* mice.

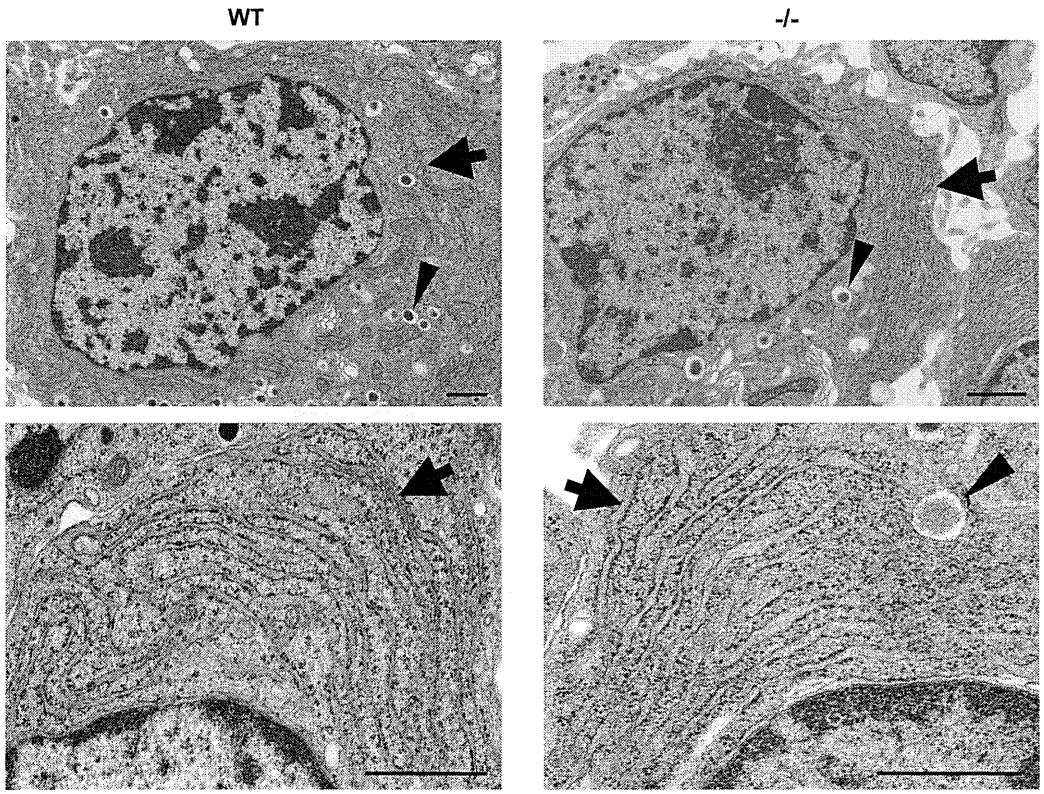

Figure S3 Ultrastructure of the rough ER in pancreatic beta cells of *Bbf2h7-/-* mice was intact. In *Bbf2h7-/-* pancreatic beta cells, the rough ER showed no morphological abnormalities. Arrows show rough ER. Arrowheads show secretory granules. Bars: 1 μm.

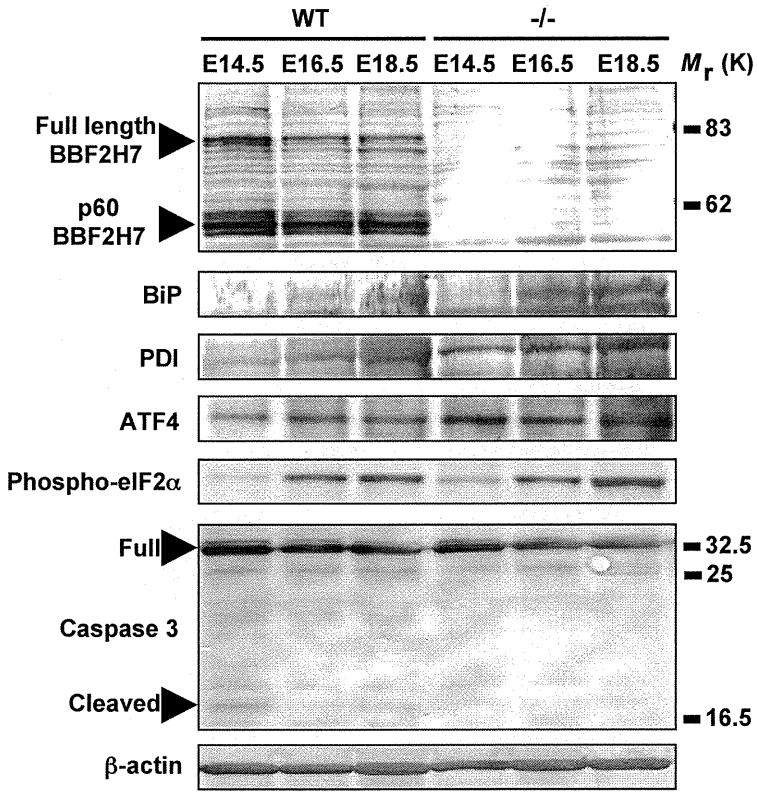

Figure S4 The expression of the ER stress-related genes was higher in *Bbf2h7-/-* mice than that of WT in the cartilage. Western blotting analysis of ER stress-related genes in rib cartilage of WT and *Bbf2h7-/-* mice. ER stress markers were gradually up-regulated in the cartilage of WT mice. The up-regulation was enhanced in *Bbf2h7-/-* mice. Note that Caspase 3 was not activated in *Bbf2h7-/-* cartilage, indicating apoptosis was not occurred.

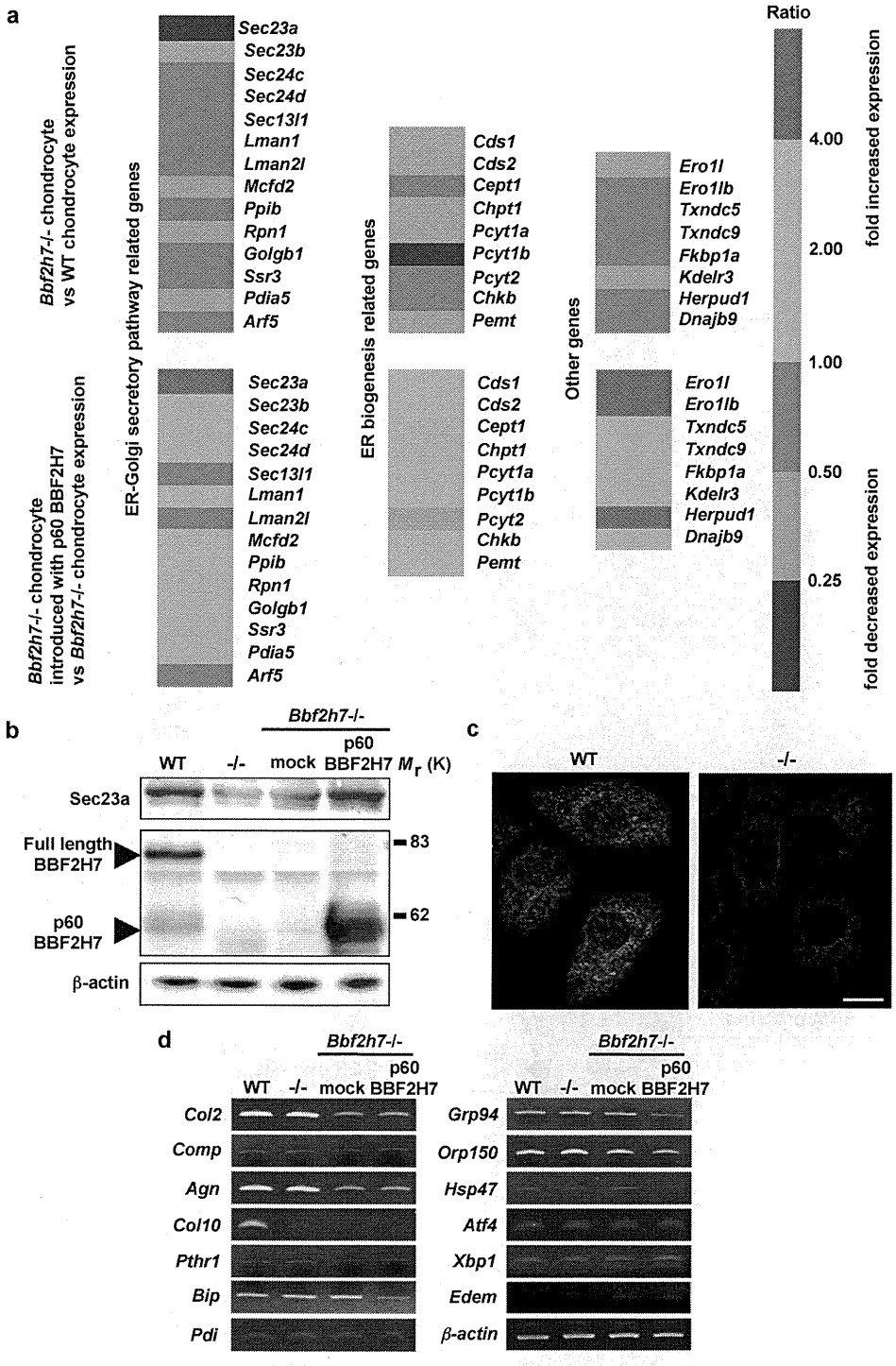

Figure S5 BBF2H7 target genes. (**a**) Microarray analysis revealed the genes down-regulated in *Bbf2h7-/-* chondrocytes included a large subset of genes encoding proteins that function in the protein secretory pathway and ER biogenesis. Almost all of these genes were up-regulated by introducing with BBF2H7 N-terminal (p60 BBF2H7) in *Bbf2h7-/-* chondrocytes. Note that *Sec23a* expression level was most down-regulated in *Bbf2h7-/-* chondrocytes and up-regulated in *Bbf2h7-/-* chondrocytes introduced with p60 BBF2H7. (**b**) Western blotting of Sec23a and BBF2H7 in primary cultured chondrocytes. Note that infection of adenovirus expressing p60 BBF2H7 restored the decreased expression of Sec23a. (**c**) Immunofluorescence of Sec23a in primary cultured chondrocytes of WT and *Bbf2h7-/-* mice. Bar: 20 μm. (**d**) Messenger RNA was extracted from primary cultured chondrocytes. These genes were not affected by infection with adenovirus expressing p60 BBF2H7.

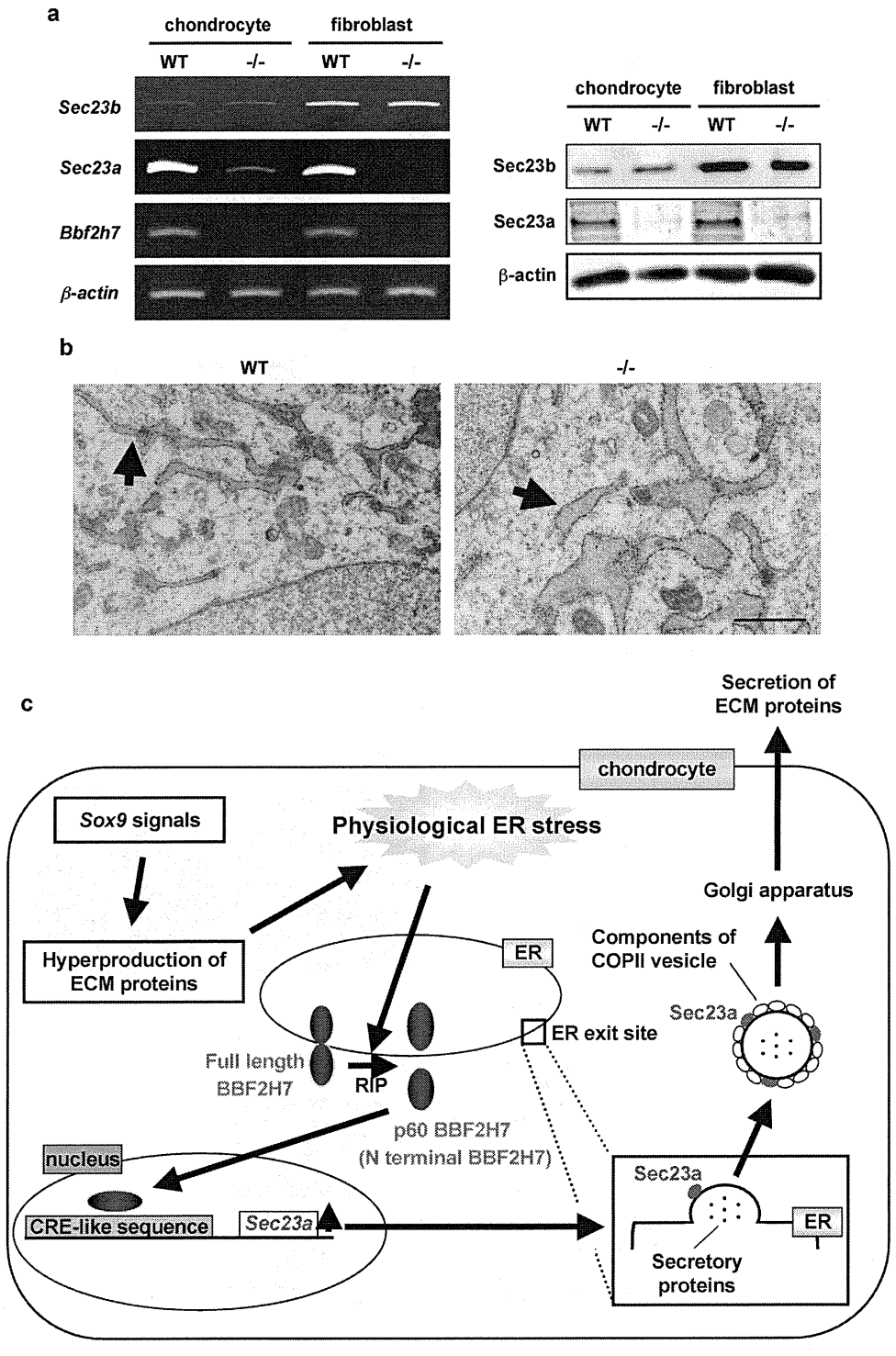

Figure S6 The expression of Sec23b and ultrastructure of rough ER in fibroblasts. (**a**) RT-PCR (left) and Western blotting (right) analysis in primary cultured chondrocytes and fibroblasts of WT and *Bbf2h7-/-* mice. The expression level of Sec23b in chondrocytes is very low. In contrast, it is much higher in fibroblasts than that of chondrocytes. (**b**) Electron microscopic analysis in primary cultured fibroblasts of WT and *Bbf2h7-/-* mice. Arrows show rough ER. In *Bbf2h7-/-* fibroblasts, the ER showed only a slight expansion of its lumen. Bar: 0.5 μm. (**c**) Proposed model for BBF2H7 mediated signaling pathway in secretion of cartilage extracellular matrix (ECM) proteins during chondrocyte differentiation.

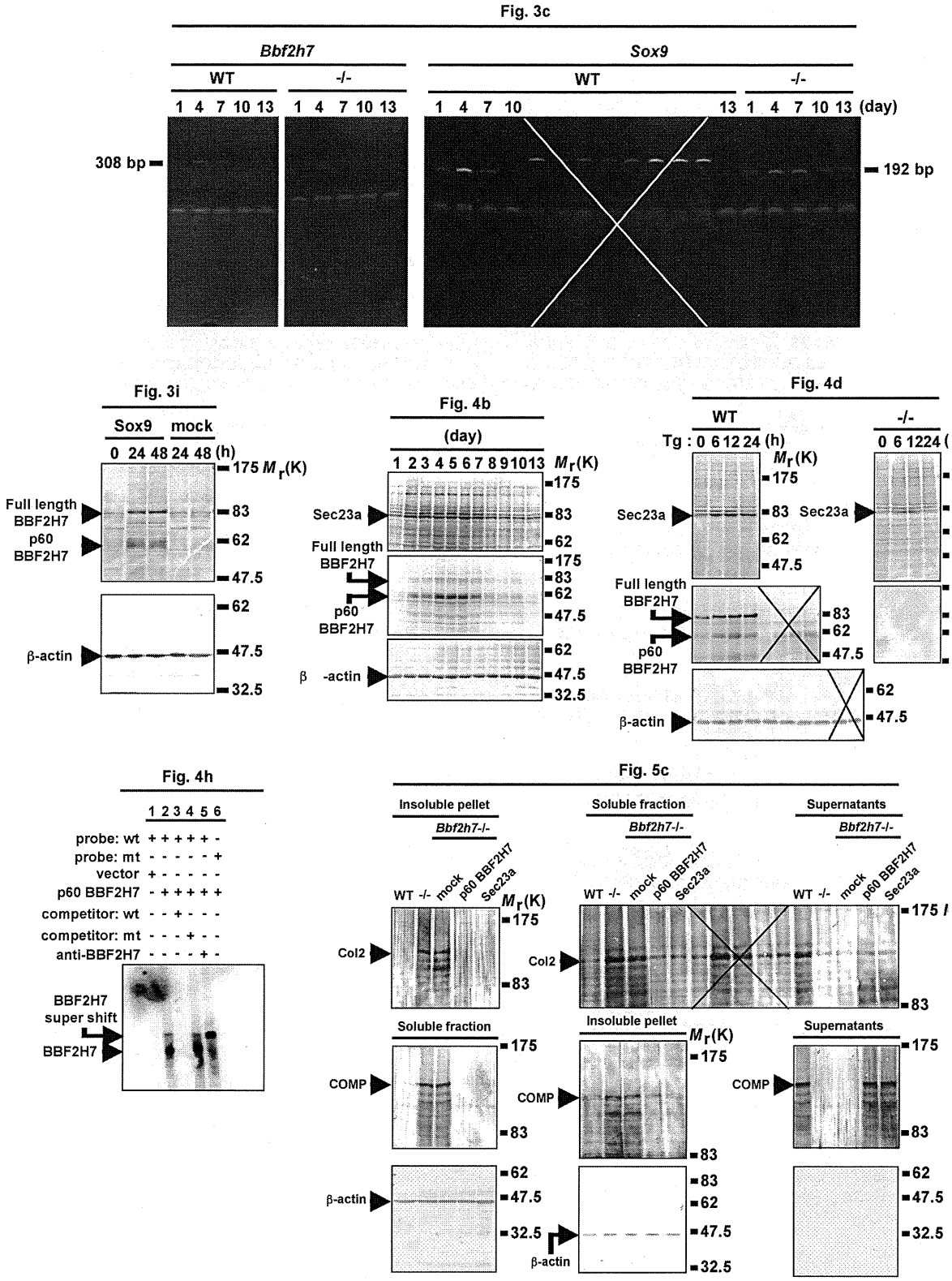

Figure S7 Full scans of key gels

Table S1 Each specific primer set using RT-PCR.

NM178661.3 360 to 667
BBF2H7-fwd GGAGCAGAGCGTCCTGCAGTG
BBF2H7-rev CCACCTCCTCGTCATTGAAGCTGTC

NM031163.2 23 to 473
procollagen2a1-fwd GGGTCTCCTGCCTCCTCCTGC
procollagen2a1-rev TCCTTTCTGCCCCTTTGGCCCTAATTTTCG

NM016685.1 362 to 681
COMP-fwd CACCGGCAACGGCTCGCACTGCACCGAC
COMP-rev CACGCCGCTGGCAGCCTGACGTCTGGTC

NM007424.2 5982 to 6220
Aggrecan-fwd GTCGGGAGCAGCAGTCACATCTGAGCAG
Aggrecan-rev CCATTCGCCTCTCTCATGCCAGATC

NM009925.3 2515 to 2723
procollagen10a1-fwd GACTCACGTTTGGGTAGGCCTG
procollagen10a1-rev CTAGGAATCCTGAGAAGGACGAGTGGAC

NM011199.1 437 to 748
PTHr1-fwd GACGCTGCGACCGCAATGGCAGCTG
PTHr1-rev GCGTGAAGCCAGAGTAGAGCACAGCGTC

NM010544.2 785 to 1120
Ihh-fwd CTCTGTCATGAACCAGTGGCCTGGTG
Ihh-rev CGGTCTCCTGGCTTTACAGCTGACAG

NM009820.2 511 to 799
Runx2-fwd CCGCACGACAACCGCACCAT
Runx2-rev CGCTCCGGCCCACAAATCTC

NM011448.3 1180 to 1371
Sox9-fwd GGACATCGGTGAACTGAGCAG
Sox9-rev GACATCCACACGTGGCCCGCGGTCGCAG

NM009825.1 897 to 1501
HSP47-fwd ACCACAGGATGGTGGACAACCGT
HSP47-rev ATCTCGCATCTTGTCTCCCTTGGG

NM022310.2 1871 to 2142
BiP-fwd GTTTGCTGAGGAAGACAAAAAGCTC
BiP-rev CACTTCCATAGAGTTTGCTGATAATTG

NM013842.2 410 to 580
XBP1-fwd ACACGCTTGGGAATGGACAC
XBP1-rev CCATGGGAAGATGTTCTGGG

NM 009716.2 833 to 1024
ATF4-fwd GGACAGATTGGATGTTGGAGAAAATG
ATF4-rev GGAGATGGCCAATTGGGTTCAC

NM 011032.2 1182 to 1264
PDI-fwd CAAGATCAAGCCCCACCTGAT
PDI-rev AGTTCGCCCCAACCAGTACTT

NM 138677.2 1085 to 1161
EDEM-fwd AAGCCCTCTGGAACTTGCG
EDEM-rev AACCCAATGGCCTGTCTGG

NM011631.1 202 to 543
GRP94-fwd GCCGAGAAGGCTCAAGGACAG
GRP94-rev CACCCGTGTCTGTGACATGCAG

NM021395.2 123 to 450
ORP150-fwd GATGTCTGTAGACCTGGGCAGTG
ORP150-rev GAACTGCAGCTGCGGACTGATCTG

NM024181.2 2716 to 2832
ERdj4-fwd CCCCAGTGTCAAACTGTACCAG
ERdj4-rev AGCGTTTCCAATTTTCCATAAATT

NM008929.2 646 to 934
P58^{IPK}-fwd GAGGTTTGTGTTTGGGATGCAG
P58^{IPK}-rev GCTCTTCAGCTGACTCAATCAG

NM009147.2 345 to 653
Sec23a-fwd GACCTACCACCCATCCAGTACGAG
Sec23a-rev CTGCATGGACTCCTTCAGAGCCTG

NM019787.3 681 to 1435
Sec23b-fwd CAGGAGATGCTGGGCCTGACCAAGTC
Sec23b-rev CCACAGATCTTCCACTGACTTGTG

NM027135.2 765 to 977
Sec24d-fwd CCGCAGATGGGAGGTGCACAGATGTC
Sec24d-rev CTCGGTGGTGACCAGTGGAGGTACCTG

XM907601.3 365 to 942
Sec31a-fwd CATCCGCTCAGCAGTTGGATGCGAC
Sec31a-rev CGCCAGCCCAGAGCAATGCATCCTG

NM007392.2 776 to 1161
β-actin-fwd TCCTCCCTGGAGAAGAGCTAC
β-actin-rev TCCTGCTTGCTGATCCACAT

Table S2 Specific probes using *in situ* hybridization.

0.5 kb fragment of mouse *Sox9* cDNA (NM011448 nucleotides 723 to 1263)

0.5 kb fragment of mouse *type II collagen* cDNA (BC051383 nucleotides 1 to 510)

0.8 kb fragment of mouse *Aggrecan* cDNA (L07049 nucleotides 1089 to 1884)

1.6 kb fragment of mouse *Ihh* cDNA (BC046984 nucleotides 663 to 2229)

0.3 kb fragment of mouse *Pthr1* cDNA (NM011199.2 nucleotides 716 to 1027)

0.6 kb fragment of mouse *type X collagen* cDNA (NM009925 nucleotides 2339 to 2955)

***Bbf2h7* probe has been described[1].**

nature
cell biology

Signalling mediated by the endoplasmic reticulum stress transducer OASIS is involved in bone formation

Tomohiko Murakami[1], Atsushi Saito[1], Shin-ichiro Hino[1], Shinichi Kondo[1], Soshi Kanemoto[1], Kazuyasu Chihara[1], Hiroshi Sekiya[1], Kenji Tsumagari[1], Kimiko Ochiai[1], Kazuya Yoshinaga[2], Masahiro Saitoh[3], Riko Nishimura[3], Toshiyuki Yoneda[3], Ikuyo Kou[4], Tatsuya Furuichi[4], Shiro Ikegawa[4], Masahito Ikawa[5], Masaru Okabe[5], Akio Wanaka[6] and Kazunori Imaizumi[1,7]

Eukaryotic cells have signalling pathways from the endoplasmic reticulum (ER) to cytosol and nuclei, to avoid excess accumulation of unfolded proteins in the ER. We previously identified a new type of ER stress transducer, OASIS, a bZIP (basic leucine zipper) transcription factor, which is a member of the CREB/ATF family and has a transmembrane domain[1–6]. OASIS is processed by regulated intramembrane proteolysis (RIP) in response to ER stress, and is highly expressed in osteoblasts. *OASIS*$^{-/-}$ mice exhibited severe osteopenia, involving a decrease in type I collagen in the bone matrix and a decline in the activity of osteoblasts, which showed abnormally expanded rough ER, containing of a large amount of bone matrix proteins. Here we identify the gene for type 1 collagen, *Col1a1*, as a target of OASIS, and demonstrate that OASIS activates the transcription of *Col1a1* through an unfolded protein response element (UPRE)-like sequence in the osteoblast-specific *Col1a1* promoter region. Moreover, expression of *OASIS* in osteoblasts is induced by BMP2 (bone morphogenetic protein 2), the signalling of which is required for bone formation. Additionally, RIP of OASIS is accelerated by BMP2 signalling, which causes mild ER stress. Our studies show that OASIS is critical for bone formation through the transcription of *Col1a1* and the secretion of bone matrix proteins, and they reveal a new mechanism by which ER stress-induced signalling mediates bone formation.

To avoid cellular damage, eukaryotic cells clear unfolded proteins from the lumen of the ER. This system is termed the unfolded protein response (UPR)[7–9]. ER stress transducers have important roles in UPR signal transduction. In mammalian cells, the three major transducers of the UPR are IRE1, PERK and ATF6. These sense unfolded proteins in the ER lumen and transduce signals to the nucleus for the transcription of UPR-target genes, the attenuation of global protein translation, and ER-associated degradation.

OASIS is structurally very similar to ATF6 (Fig. 1a). I*n situ* hybridization with various tissues and organs of postnatal mice, showed the most intense *OASIS* mRNA signals along cortical and trabecular bones (Fig. 1b), corresponding to mRNA signals of *Col1a1*, which is expressed in osteoblasts (Fig. 2d)[10]. Moreover, *OASIS* mRNA was highly expressed in primary osteoblasts, but not in primary osteoclasts (Fig. 1c).

To assess the *in vivo* role of OASIS, we generated *OASIS*$^{-/-}$ mice by homologous recombination (Supplementary Information, Fig. 1a–c). *OASIS*$^{-/-}$ mice were born at the expected Mendelian ratios, but showed growth retardation (Supplementary Information, Fig. 1d). Focal swellings of limbs or heels due to fractures were often observed macroscopically. Radiographs and micro-computed tomography (μCT) analyses revealed a decrease in bone density at all skeletal sites in *OASIS*$^{-/-}$ mice compared with wild type (Fig. 1d). These findings indicate that the skeleton of *OASIS*$^{-/-}$ mice was extremely fragile.

Hematoxylin-eosin-stained sections of osseous tissues revealed that both cortical and trabecular bones in the femur of *OASIS*$^{-/-}$ mice were much thinner than those of wild-type mice (Fig. 1e). In contrast, the epiphyseal growth plate and cartilage tissue of *OASIS*$^{-/-}$ mice were not affected (Fig. 1e). Bone densitometry and μCT analysis showed that the bone mineral density of *OASIS*$^{-/-}$ mice was decreased from the proximal to the distal division, and that trabecular bone was thin in the femurs (Fig. 1f). Histomorphometric analyses revealed that both bone volume/tissue volume (BV/TV) and trabecular thickness (Tb.Th) were decreased in *OASIS*$^{-/-}$ mice, whereas the trabecular number (Tb.N, the number of trabecular bones in measured tissue area) was not altered (Fig. 1g). Other parameters associated with osteogenesis were also reduced (Fig. 1h, Supplementary Information, Fig. 1e, f). In contrast,

[1]Division of Molecular and Cellular Biology, Department of Anatomy, Faculty of Medicine, University of Miyazaki, 5200 Kihara, Kiyotake, Miyazaki 889-1692, Japan. [2]Department of Anatomy and Pathology, Kumamoto University School of Health Sciences, 4-24-1 Kuhonji, Kumamoto 862-0976, Japan. [3]Department of Molecular and Cellular Biochemistry, Graduate School of Dentistry, Osaka University, 1-8 Yamadaoka, Suita, Osaka 565-0871, Japan. [4]Laboratory for Bone and Joint Diseases, RIKEN SNP Research Center, 4-6-1 Shirokanedai, Minato-ku, Tokyo 108-8639, Japan. [5]Genome Information Research Center and Graduate School of Pharmaceutical Sciences, Osaka University, 3-1 Yamadaoka, Suita, Osaka 565-0871, Japan. [6]Department of Anatomy and Neuroscience, Nara Medical University, 840 Shijo-cho, Kashihara, Nara 634-8521, Japan.
[7]Correspondence should be addressed to K.I. (e-mail: imaizumi@med.miyazaki-u.ac.jp).

Received 12 June 2009; accepted 27 August 2009; published online 20 September 2009; DOI: 10.1038/ncb1963

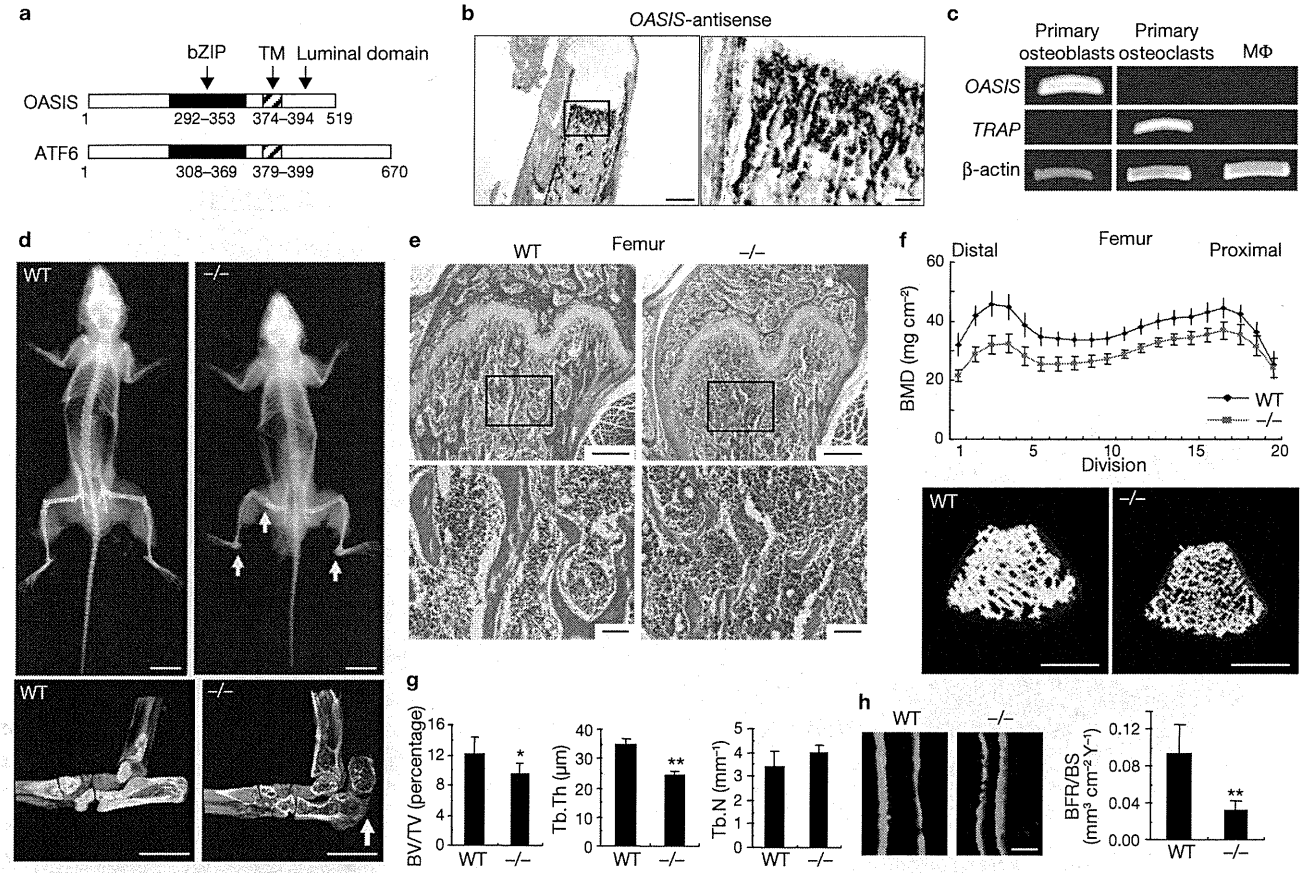

Figure 1 *OASIS*$^{-/-}$ mice exhibit severe osteopenia. (**a**) Predicted peptide features of human OASIS and ATF6. The basic leucine zipper (bZIP), putative transmembrane domain (TM) and luminal domain are indicated. (**b**) *In situ* hybridization analysis of mouse tibia at postnatal day 4 (P4) using *OASIS*-antisense probes. Scale Bar, 500 μm. Right, higher magnification of the framed area on the left. Scale Bar, 100 μm. (**c**) RT-PCR analysis of *OASIS* and *TRAP* (marker of osteoclasts) in primary osteoblasts, osteoclasts and macrophages (MΦ). (**d**) Radiographs of 12-week-old wild-type and *OASIS*$^{-/-}$ male mice. Spontaneous fractures in the *OASIS*$^{-/-}$ mouse are indicated by arrows (upper panels). Scale Bar, 1 cm. μCT analysis of heels (lower panels) show decreased cortical bones and a calcaneus fracture (arrow) in the *OASIS*$^{-/-}$ mouse. Scale bars, 2 mm. (**e**) Hematoxylin- eosin staining of femurs in wild-type and *OASIS*$^{-/-}$ mice. Lower panels (scale bar, 100 μm) are a higher magnification of the framed areas in the upper panels (Scale bar, 500 μm). (**f**) Bone mineral densities (BMD) of femurs were measured in 20 longitudinal divisions (12-week-old male, mean ± s.d., $n = 6$; divisions 1–18, $P < 0.01$; division 19, $P < 0.05$; Student's *t*-test). Lower panels show μCT analysis of trabecular bones in femurs. Scale bars, 1 mm. (**g**) Histomorphometric analyses of bone volume/tissue volume (BV/TV), trabecular thickness (Tb.Th) and trabecular number (Tb.N) in *OASIS*$^{-/-}$ mice (mean ± s.d., $n = 5$, $^{*}P < 0.05$, $^{**}P < 0.01$; Student's *t*-test). (**h**) Calcein double labelling of tibiae in wild-type and *OASIS*$^{-/-}$ mice. Right panel shows that the bone formation rate/bone surface (BFR/BS) is significantly reduced in *OASIS*$^{-/-}$ mice (mean ± s.d., $n = 5$, $^{**}P < 0.01$, Student's *t*-test). Scale Bar, 5 μm). WT, wild type; –/–, *OASIS*$^{-/-}$.

the eroded surface (eroded surface/bone surface, ES/BS) was normal in *OASIS*$^{-/-}$ mice with no significant change in osteoclast surface/bone surface (Oc.S/BS) between wild-type and *OASIS*$^{-/-}$ mice, and *OASIS* mRNA was not expressed in osteoclasts (Fig. 1c, Supplementary Information, Fig. 1h). Levels of osteoprotegerin and RANKL in *OASIS*$^{-/-}$ osteoblasts were equal to those in wild-type osteoblasts (Supplementary Information, Fig. 1i). The numbers of CFU-F and CFU-ALP (colony-forming units, fibroblast and alkaline phosphatase-positive) were not changed in cultures of *OASIS*$^{-/-}$ bone stromal cells compared with in those of wild-type cells, but the number of CFU-O (osteoblasts) was significantly reduced (Supplementary Information, Fig. 1g), indicating that maturation was delayed in *OASIS*$^{-/-}$ osteoblasts, although differentiation in the early stages in osteoblasts was normal. These results suggest that osteopenia in the osseous tissues of *OASIS*$^{-/-}$ mice is a result of decreased bone formation, associated with a delay in osteoblast maturation, and not with increased bone resorption.

Electron microscopic analysis using ultra-thin sections of tibiae revealed that the osteoblasts of *OASIS*$^{-/-}$ mice contained abnormally enlarged rough ER (Fig. 2a). In contrast, this was not observed in osteocytes, osteoclasts or chondrocytes of *OASIS*$^{-/-}$ mice (Supplementary Information, Fig. 2). Immunohistochemistry showed that bone matrix proteins, such as procollagen 1a1 and osteocalcin (Ocn), were accumulated in the expanded rough ER of *OASIS*$^{-/-}$ osteoblasts (Fig. 2b). Thus, we concluded that an osteoblast dysfunction that prevents the secretion of bone matrix proteins from osteoblasts could contribute to severe osteopenia in *OASIS*$^{-/-}$ mice.

To gain further insight into the potential mechanisms underlying defective bone formation in *OASIS*$^{-/-}$ mice, we compared gene expression in calvaria of wild-type and *OASIS*$^{-/-}$ mice at postnatal day 4 using a microarray. We found that *Col1a1* and *Col1a2* mRNAs were downregulated, and expression of *Ocn*, osteopontin (*Opn*), bone sialoprotein (*Bsp*) and alkaline phosphatase (*Alp*) mRNAs were upregulated, in the bone tissue of *OASIS*$^{-/-}$ mice. Reverse transcription (RT)-PCR showed that *Col1a1* and *Col1a2* mRNAs were downregulated by 30–40%, and *Ocn*, *Opn*, *Bsp* and *Alp* mRNAs were upregulated by 50–70% (Fig. 2c,

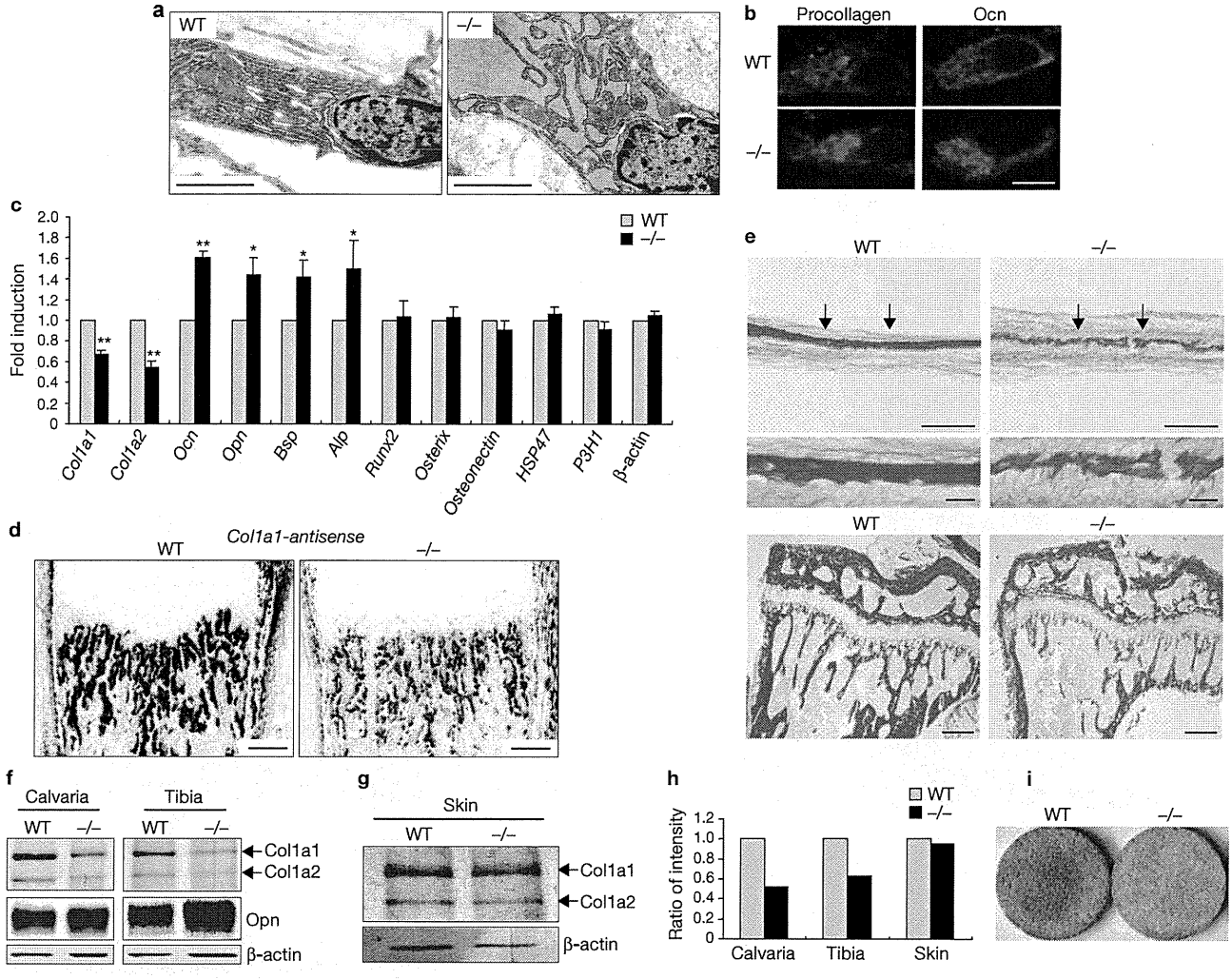

Figure 2 Abnormal expansion of rough ER with accumulation of bone matrix proteins in *OASIS*$^{-/-}$ osteoblasts and decreased expression of *Col1* mRNAs in *OASIS*$^{-/-}$ bone tissue. (**a**) Electron microscopic images of tibiae from 4-month-old wild-type and *OASIS*$^{-/-}$ female mice. Scale bars, 2 μm. (**b**) Immunohistochemistry using anti-procollagen 1a1 (LF41) and anti-osteoclacin (Ocn) antibodies in wild-type and *OASIS*$^{-/-}$ osteoblasts from calvaria at postnatal day 4 (P4). Scale bar, 5 μm. Note that both proteins accumulate in the ER of *OASIS*$^{-/-}$ osteoblasts. (**c**) Quantitative analysis of RT-PCR using RNA from P4 calvaria of wild-type and *OASIS*$^{-/-}$ mice (mean ± s.d., $n = 3$, $^{*}P < 0.05$, $^{**}P < 0.01$; Student's *t*-test). (**d**) *In situ* hybridization analysis of *Col1a1* using P4 tibiae. Scale bar, 200 μm. (**e**) Van Gieson staining (specifically stains collagen fibrils) of calvaria (upper panels: P4; scale bars, 100 μm) and tibiae (lower panels: 3-month-old females; scale bars, 500 μm) in wild-type and *OASIS*$^{-/-}$ mice. Arrows indicate flat calvaria bones. The regions between the arrows are magnified in the middle panel (scale bar, 20 μm). Note the dramatic decrease of collagen fibrils content in *OASIS*$^{-/-}$ mice compared with wild type. (**f, g**) Electrophoretic analysis of type I collagen (Col1a1 and Col1a2) using protein extracted from P4 calvaria, tibiae (**f**) and skins (**g**) of wild-type and *OASIS*$^{-/-}$ mice. (**h**) Quantitative analysis of Col1 in **f** and **g**. (**i**) Van Gieson staining of primary cultured osteoblasts from wild-type and *OASIS*$^{-/-}$ mice on hydroxyapatite scaffolds. WT, wild type; −/−, *OASIS*$^{-/-}$.

Supplementary Information, Fig. 3a, b). In cultured osteoblasts, *Col1a1* and *Col1a2* mRNAs were also significantly downregulated, and *Ocn* and *Bsp* mRNAs upregulated (Supplementary Information, Fig. 3c). *In situ* hybridization and van Gieson staining of tissue sections from the tibia and calvaria showed that *Col1a1* mRNA and type I collagen protein were markedly decreased in *OASIS*$^{-/-}$ mice (Fig. 2d, e). Similar results were obtained by electrophoretic analysis of type I collagen using protein extracted from these bones and by van Gieson staining of primary cultured osteoblasts (Fig. 2f, h, i). In contrast, the level of type I collagen in the skin of *OASIS*$^{-/-}$ mice was almost equal to that in wild-type mice (Fig. 2g, h), indicating that type I collagen was specifically decreased in the bone matrix of *OASIS*$^{-/-}$ mice and the bone quality of *OASIS*$^{-/-}$ mice was not healthy. Most genes essential for osteoblast differentiation, such as *Runx2* and *Osterix*[11–14], and for collagen folding, such as *HSP47* (ref. 15) and prolyl 3-hydroxylase 1 (*P3H1*; refs 16, 17), were not affected in *OASIS*$^{-/-}$ mice (Supplementary Information, Fig. 3a). Moreover, the expression of ER stress-related genes, such as *BiP*, *CHOP*, *ATF4* and *EDEM*, was also unchanged in the bone tissues and primary osteoblasts in *OASIS*$^{-/-}$ mice relative to those in wild-type (Supplementary Information, Fig. 4).

We next examined changes in expression of *Col1a1* and *Col1a2* in MC3T3-E1 cells infected with an adenovirus expressing *OASIS*. Both *Col1a1* and *Col1a2* were upregulated by overexpression of OASIS (Fig. 3a; Supplementary Information, Fig. 5a). In contrast, no changes were observed in *Ocn*, *Opn*, *Bsp*, and *Alp* (Supplementary Information, Fig. 5b). Infection of *OASIS*$^{-/-}$ osteoblasts with an adenovirus expressing

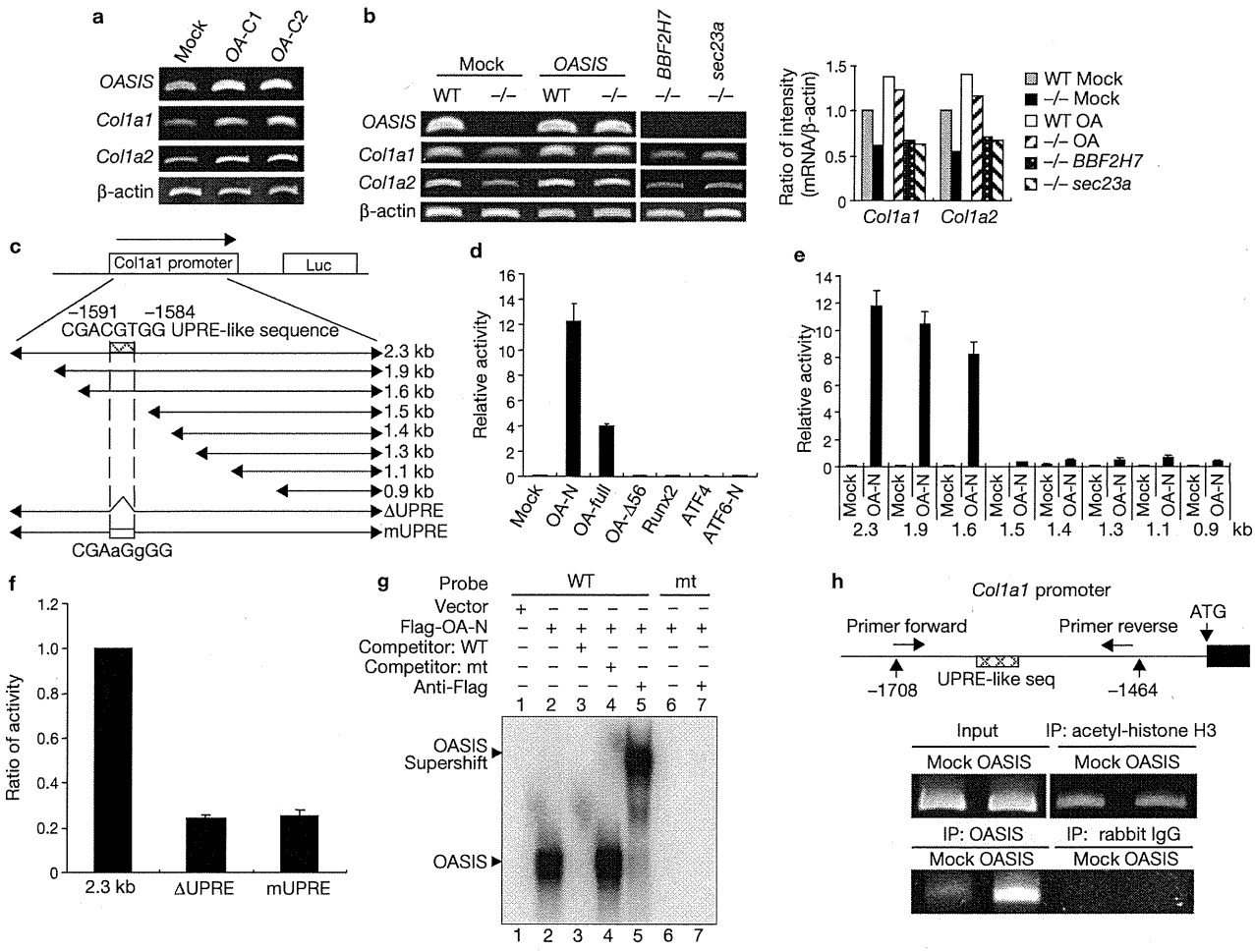

Figure 3 OASIS promotes *Col1a1* transcription through a UPRE-like sequence. (**a**) RT-PCR analysis of *Col1a1* and *Col1a2* from MC3T3-E1 cells infected with an adenovirus (ad) expressing *OASIS* (ad-OASIS). *OA*-C1 and *OA*-C2, adenoviruses expressing *OASIS* clone 1 and clone 2, respectively. (**b**) Left, RT-PCR analysis of primary osteoblasts infected with ad-*OASIS*, ad-*BBF2H7* or ad-*sec23a*. Right, quantitative analysis of the expression levels in the left panel. (**c**) Schematic representations of reporter plasmids of the mouse 2.3 Kb *Col1a1* promoter and nine mutations. The locations of the UPRE-like sequence are indicated. ΔUPRE lacks a UPRE-like sequence, and mUPRE has a mutated sequence. (**d**) Reporter assays using the 2.3-kb *Col1a1* promoter. MC3T3-E1 cells were transfected with the indicated plasmids and the pGL3-*Col1a1* promoter (2.3 kb). Data are presented as the ratio of firefly luciferase activity to *Renilla* luciferase activity. (**e**, **f**) Reporter assays using deletion constructs of the *Col1a1* promoter (**e**), ΔUPRE or mUPRE (**f**) with an OA-N expression vector. (**g**) The labelled UPRE-like sequence was incubated with an *in vitro* translated OASIS N-terminal fragment tagged with Flag (Flag-OA-N). Note that the binding was abolished by incubation with an unlabelled competitor (lane 3), but not by a competitor mutated from CGACGTGG to CGAaGggGG (mt, lane 4). The addition of an anti-Flag antibody caused a supershift in mobility (lane 5). Direct binding by a labelled mutant probe was not detected (lane 6, 7). (**h**) Upper panel, schematic representation of the *Col1a1* promoter and the annealing sites of the primer set. Lower panel, MC3T3-E1 cells infected with the indicated adenovirus were subjected to ChIP assays using each antibody. Luc; luciferase; OA, OASIS; OA-N, N-terminal fragment of Oasis; OA-full, full-length OASIS; OA-Δ56, dominant-negative form of OASIS; ATF6-N, active form of ATF6; Mock, empty vector; WT, wild type; -/-, *OASIS*$^{-/-}$. Data in **d**–**f** are mean ± s.d., n = 6.

OASIS recovered expression levels of *Col1a1* and *Col1a2* mRNA (Fig. 3b). An active form of BBF2H7, which is structurally very similar to OASIS and is expressed in chondrocytes[18], could not induce *Col1a1* and *Col1a2* mRNA, suggesting that *Col1a1* and *Col1a2* induction by OASIS is specific and that they could be direct targets of OASIS. Upregulation of mature osteoblast markers, including *Ocn* and *Bsp* (Fig. 2c; Supplementary Information, Fig. 3c), was considered to occur secondary to defective bone matrix production in OASIS$^{-/-}$ osteoblasts, as the introduction of OASIS did not affect the expression levels of these genes. The details of the mechanisms upregulating these markers in *OASIS*$^{-/-}$ osteoblasts remain unclear. It is possible that this upregulation may occur as part of a compensatory response to decreased production and secretion of bone matrix proteins. ATF4 is known to be involved in the regulation of *Ocn* and *Bsp* gene expression, and also in collagen synthesis[19]. Therefore, upregulation of *Ocn* and *Bsp* may be due to transcriptional promotion by ATF4 in response to decreased levels of collagen in *OASIS*$^{-/-}$ osteoblasts.

To investigate the regulatory mechanisms underlying *Col1a1* transcription by OASIS, we performed reporter assays using a reporter gene carrying a 2.3-kb promoter of *Col1a1*, which is an osteoblast-specific regulatory region (Fig. 3c)[20,21]. Reporter activities in MC3T3-E1 cells transfected with an expression vector for full-length OASIS (OA-full) or the amino-terminal portion of OASIS (OA-N), a bioactive fragment that includes the transcriptional activation and DNA-binding domains, were significantly induced compared with mock-transfected controls (Fig. 3d). In contrast, reporter activities in cells transfected with a dominant-negative form of OASIS (OA-Δ56; ref. 2), Runx2, ATF4 (ref. 19), or an active form of ATF6

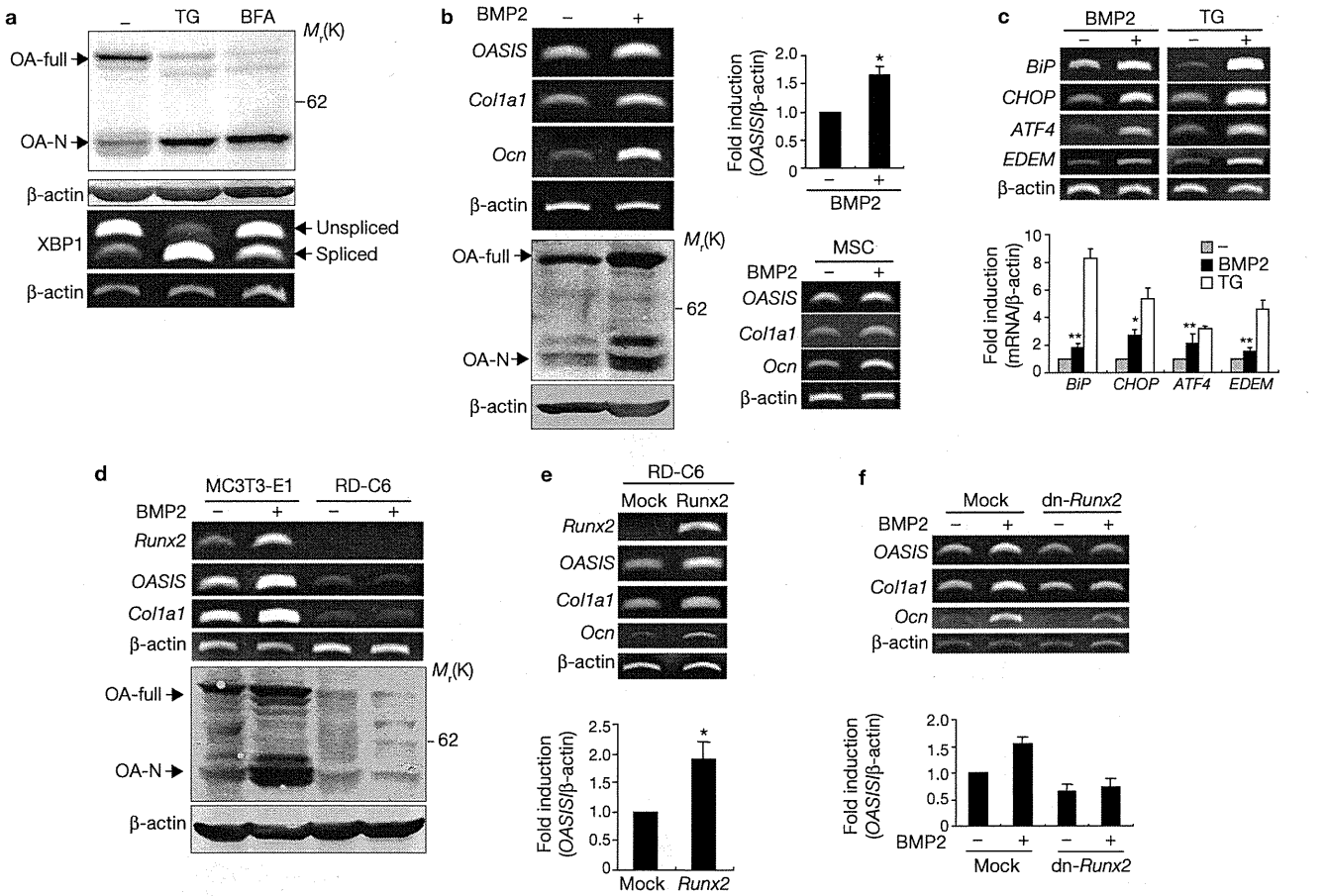

Figure 4 Features of OASIS expression in osteoblasts. (**a**) MC3T3-E1 cells were treated for 2 h with thapsigargin (TG; 1 μM) or brefeldin A (BFA; 1 μg ml^{-1}) and MG132 (5 μM) to suppress degradation of the cleaved N-terminal OASIS fragments. Upper panels show immunoblotting of OASIS. Lower panels show RT-PCR of *XBP1* mRNA. When cells were exposed to ER stressors, the amounts of full-length OASIS decreased and OA-N severely accumulated. (**b**) RT-PCR (upper left) and western blotting (lower left) of OASIS in primary calvarial osteoblasts treated with BMP2 (100 ng ml^{-1}) for 5 days . Upper right, quantitative analysis of *OASIS* mRNA (mean ± s.d., $n = 3$, $^*P < 0.01$; Student's *t*-test). Lower right, RT-PCR analysis in primary cultures of bone marrow stromal cells (MSCs) treated with BMP2 (100 ng ml^{-1}) for 5 days. *OASIS* mRNA was induced in calvarial osteoblasts and MSCs by BMP2. (**c**) RT-PCR analysis of UPR-related genes in primary osteoblasts treated with BMP2 (100 ng ml^{-1}) for 5 days or thapsigargin (TG; 1 μM) for 6 h. Lower panels, quantitative analysis of each mRNA level (mean ± s.d., $n = 3$, $^*P < 0.01$, $^{**}P < 0.05$; Student's *t*-test). (**d**) RT-PCR (upper panel) and western blotting (lower panel) of OASIS in MC3T3-E1 and *Runx2*-deficient (RD-C6) cells treated with BMP2 (100 ng ml^{-1}) for 5 days. (**e**) RT-PCR analysis of *OASIS* in RD-C6 cells infected with an adenovirus expressing *Runx2*. Lower panel, quantitative analysis of *OASIS* mRNA levels (mean ± s.d., $n = 3$, $^*P < 0.01$; Student's *t*-test). Overexpression of *Runx2* promoted the expression of *OASIS* with the inductions of Runx2 target genes such as *Ocn* and *Col1a1* in RD-C6 cells. (**f**) RT-PCR analysis of *OASIS* in MC3T3-E1 cells infected with an adenovirus expressing dominant negative (dn)-*Runx2* and then treated with BMP2 for 5 days BMP2 (100 ng ml^{-1}). Lower panels, quantitative analysis of *OASIS* mRNA levels (mean ± s.d., $n = 3$). Note that the inductions of OASIS and Runx2 target genes such as *Col1a1* and *Ocn* after BMP2 treatment were suppressed by dn-*Runx2*. ; OA-N, N-terminal fragment of Oasis; OA-full, full-length OASIS; Mock, empty vector; WT, wild type.

(ATF6-N) were not induced. Reporter activities in cells transfected with 1.5-kb mutants were significantly reduced (Fig. 3e), indicating that the cis-elements in the *Col1a1* promoter, on which OASIS acts, could lie in the region between 1.5 and 1.6 kb.

Using the Match program, we identified a UPRE (unfolded protein response element; TGACGTGG)[22]-like sequence (CGACGTGG) that is conserved among humans, mice and rats, and lies in the 1.5 to 1.6-kb region. We previously reported that OASIS can bind to CRE (cyclic AMP responsive element; TGACGTCA)[2], which is similar to the UPRE-like sequence. Reporter activities in cells transfected with the mutant reporter constructs ΔUPRE and mUPRE were dramatically reduced (Fig. 3f). By electrophoretic mobility shift assays we detected Flag-tagged OASIS bound to the UPRE-like sequence, but not to a mutant one (Fig. 3g). Chromatin immunoprecipitation (ChIP) assays revealed that OASIS binds to the promoter region of endogenous *Col1a1* in MC3T3-E1 cells (Fig. 3h). Thus, we concluded that OASIS directly binds to the UPRE-like sequence in the *Col1a1* promoter region to induce its transcription in osteoblasts.

Next, we investigated the expression of OASIS under various conditions in osteoblasts. Western blot and RT-PCR analysis of extracts from MC3T3-E1 cells showed small amounts of OA-N and spliced forms of *XBP1* (an indicator of ER stress) mRNA under normal conditions (Fig. 4a), indicating that weak ER stress occurs in osteoblasts under normal conditions. When MC3T3-E1 cells were exposed to ER stress, OASIS was dramatically processed by RIP (Fig. 4a) and OA-N was translocated to nuclei (Supplementary Information, Fig. 5c), indicating that OASIS is activated by ER stress in osteoblasts as well as other cells such as astrocytes. Interestingly, treatment with BMP2, which is required for

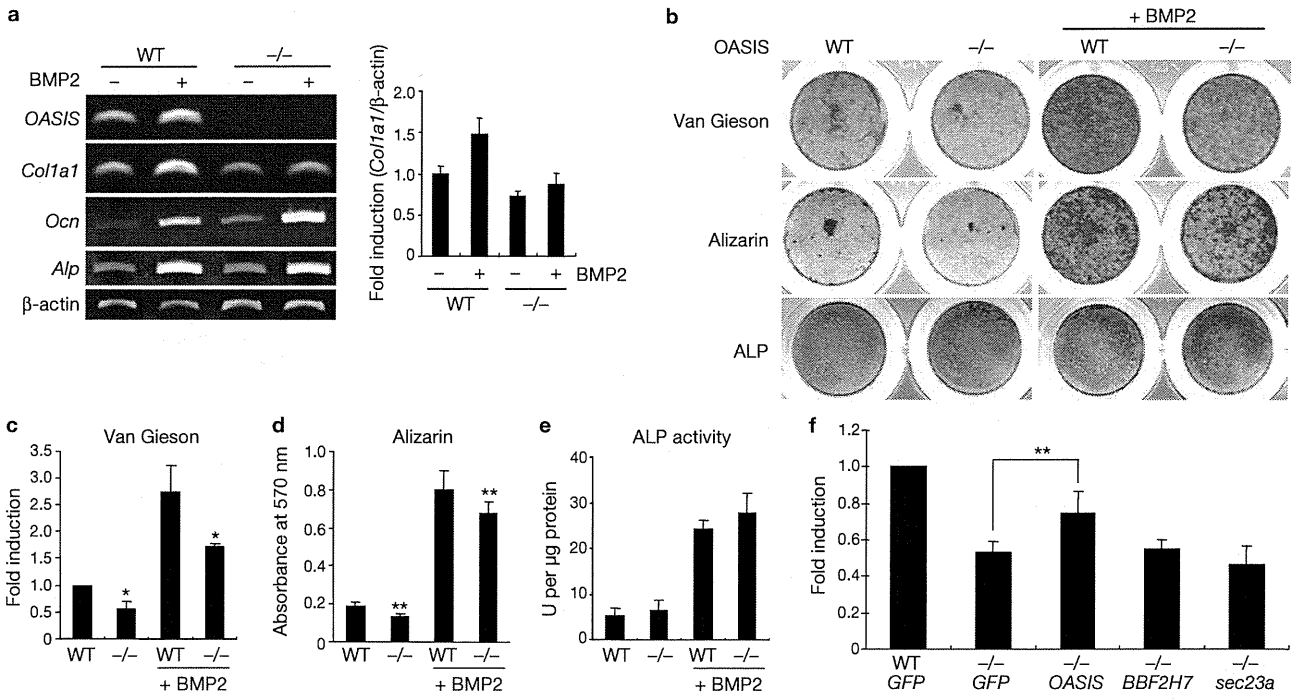

Figure 5 The functions of OASIS are essential for osteogenesis. (**a**) The expression level of *Col1a1*, *Ocn*, and *Alp* mRNAs in wild-type and *OASIS*$^{-/-}$ primary osteoblasts treated with BMP2 (100 ng ml^{-1}) for 5 days (mean ± s.d., $n = 3$). Right panel, quantitative analysis of *Col1a1* mRNA levels. Note that the induction of *Col1a1* mRNA by treatment with BMP2 was suppressed in *OASIS*$^{-/-}$ osteoblasts, whereas *Ocn* and *Alp* mRNAs were sufficiently induced. (**b**–**e**) Wild-type and *OASIS*$^{-/-}$ osteoblasts were cultured with ascorbic acid and β-glycerophosphate, with or without BMP2 (100 ng ml^{-1}) for a week. Cultures were stained with van Gieson for detection of collagen fibrils, alizarin red S for mineralization and nitro blue tetrazolium and 5-bromo-4-chroro-3-indolyl phosphate for alkaline phosphatase (ALP) activities (**b**). *OASIS*$^{-/-}$ cultures showed declined mineralization with the decrease of collagen fibrils in the absence or presence of BMP2. Quantitative analyses of van Gieson (**c**), alizarin red S (**d**) and ALP activities (**e**). Asterisks indicate a significant difference from each wild type (mean ± s.d., $n = 4$, $^{*}P < 0.01$, $^{**}P < 0.05$; Student's *t*-test). (**f**) Quantitative analysis of van Gieson staining on primary osteoblasts infected with an adenovirus expressing *GFP*, *OASIS*, *BBF2H7* or *sec23a*. Wild-type and *OASIS*$^{-/-}$ osteoblasts were cultured with ascorbic acid, β-glycerophosphate and BMP2 (100 ng ml^{-1}) for a week. Cultures were stained with van Gieson and then the intensities were measured (mean ± s.d., $n = 4$, $^{**}P < 0.05$; Student's *t*-test). WT, wild type; −/−, *OASIS*$^{-/-}$.

bone formation and osteoblast differentiation[23], induced the expression of *OASIS* mRNA in calvarial osteoblasts and bone marrow stromal cells, and accelerated RIP of OASIS and nuclear translocation of OA-N in osteoblasts (Fig. 4b; Supplementary Information, Fig. 5c). As OASIS is cleaved in response to ER stress, it is possible that RIP of OASIS by BMP2 is mediated by ER stress. We examined whether BMP2 induces ER stress in osteoblasts. The expression levels of ER stress markers, *BiP*, *CHOP*, *ATF4* and *EDEM*, were slightly but significantly upregulated by BMP2 stimulation (Fig. 4c). These findings suggest that the BMP2 signalling pathway can induce mild ER stress in osteoblasts and that OASIS is activated in response to ER stress, and transduces signals to the nucleus for osteogenesis. When differentiating into their mature form, osteoblasts produce abundant proteins and parts of these would be transiently accumulated in the ER. Thus, it is possible that ER stress in osteoblasts treated with BMP2 is associated with a high demand for synthesis and secretion of bone matrix proteins. Similar phenomena are also seen during differentiation of plasma cells[24], which synthesize and secrete abundant antibodies. For the full development of secretory machinery in plasma cells, activation of ER stress signalling is essential.

BMP2 has been reported to require the transcription factor Runx2 for induction of osteoblast differentiation[11,12,23]. We investigated the requirement for Runx2 in OASIS activation after treatment with BMP2 in osteoblasts. The expression levels of *OASIS* mRNA and protein was extremely low and RIP of OASIS by BMP2 was not induced, in *Runx2*-deficient RD-C6 cells[25] (Fig. 4d). Moreover, overexpression of *Runx2* promoted the expression of *OASIS* mRNA in RD-C6 cells (Fig. 4e), and the induction of *OASIS* mRNA after BMP2 treatment was inhibited in MC3T3-E1 cells infected with an adenovirus expressing dominant-negative *Runx2* (Fig. 4f), indicating that expression and induction of OASIS could be downstream of Runx2.

Treatment with BMP2 induced expression of *Col1a1* mRNA in wild-type cells (Fig. 5a); in contrast, the induction was significantly inhibited in *OASIS*$^{-/-}$ cells although *Ocn* and *Alp* mRNAs were sufficiently induced, suggesting that OASIS is essential for *Col1a1* mRNA induction by BMP2. Furthermore, *OASIS*$^{-/-}$ osteoblast cultures showed a decrease in collagen fibres and delayed mineralized nodule formation relative to wild-type cultures, both in the absence and presence of BMP2, although alkaline phosphatase activity showed no difference between the two cultures (Fig. 5b–e). The decrease in collagen fibres in a culture of *OASIS*$^{-/-}$ osteoblasts was recovered by the introduction of OASIS (Fig. 5f). Taken together, these results suggested that the functions of OASIS are essential for osteogenesis.

From this study, we conclude that OASIS plays a critical role in bone formation through the transcription of *Col1a1* and the secretion of bone matrix proteins. A putative model of the OASIS-mediated signalling pathway from BMP2 to bone formation is shown in Supplementary Information, Fig. 6. Our results indicate that ER stress response has important roles not